Disentangling mechanical and sensory modules in the radiation of Noctilionoid bats

Abstract

The vertebrate cranium is a complex anatomical structure with diverse mechanical and sensory functions. Shifts between modularity and integration in both sets of functions, especially mechanical function, have been implicated in adaptive diversification. However, how mechanical and sensory systems and functions have coevolved and how their interrelationship contributes to phenotypic disparity remains largely unexplored. To examine the modularity, integration and evolutionary rates of sensory and mechanical structures within the head, we analyzed hard and soft tissue scans from ecologically diverse bats from the superfamily Noctilionoidea, which range from generalized insectivores to derived frugivores and nectarivores. We identified eight cranial regions as distinct modules — five associated with bite force and three linked to the olfactory, visual, and auditory systems, respectively — whose interrelationships differ between Neotropical leaf-nosed bats (Family Phyllostomidae) and other noctilionoids. Our analyses suggest that the peak rates of sensory module evolution predate those of mechanical modules. This finding is consistent with transitions to new diets first involving changes in the detection of novel food items, followed by adaptations to process them. We propose the coevolution of structures influencing bite force, olfaction, vision, and hearing constituted a *structural* opportunity that allowed the phyllostomid ancestor to take advantage of existing *ecological* opportunity and the group to become a classic example of adaptive radiation.

Key Words:

Cranium, Integration, Modularity, Sensory, Trait relationships

Introduction

How multiple traits are organized and re-organized, and how that organization impacts the nature of evolutionary change, are outstanding questions in biology (Esteve-altava 2017). Among vertebrates, the morphology of the cranium is compartmentalized into numerous semi-autonomous modules that display strong internal correlation relative to their correlation with other modules, with some of these correlations being likely conserved across mammals (Atchley and Hall 1991; Goswami 2006; Porto et al. 2009; Goswami and Polly 2010; Assis et al. 2016; Goswami and Finarelli 2016; Evans et al. 2017; Felice and Goswami 2017; Bardua et al. 2019). The impact of this modularity on the nature of morphological evolution remains a source of significant, ongoing inquiry. Studies have linked higher evolvability and increased phenotypic diversity to the boundaries prescribed by highly integrated modules (Esteve-altava 2017; Felice et al. 2018; Hedrick et al. 2020), while others have found that modularity influences the direction of evolutionary change but not its rate (Goswami et al. 2014; Conith et al. 2019; Rossoni et al. 2019; Watanabe et al. 2019). Moreover, despite the importance of sensory information to organismal function and the obvious physical and functional links between sensory and mechanical systems in the vertebrate skull, the modularity of cranial sensory systems and their relationship to mechanical modules has not been explicitly investigated. In this study, we take advantage of recent advances in iodine staining in conjunction with high-resolution computed tomography (CT) (Gignac et al. 2016; Hedrick and Dumont 2018; Yohe et al. 2018; Camilieri-Asch et al. 2020) to quantify soft-tissue sensory structure shape and volume

44 and use the resulting data to test hypotheses about sensory and mechanical modules in the
45 cranium and evaluate their relationship across evolutionary time.
46 Modularity in mature organisms results from the accumulated products of processes
47 acting at many different biological scales. During development, genetically defined modules
48 change over time due to pleiotropy, linkage disequilibrium, environmental stimuli, physical
49 interactions among modules and selection (Wagner and Altenberg 1996; Klingenberg et al.
50 2004; Klingenberg 2010; Clune et al. 2013; Assis et al. 2016). Because of these diverse
51 processes, developmental modules are frequently unrecoverable in adult forms. Indeed, a
52 recent analysis of adult cichlids provides evidence of stronger associations among different
53 functional modules (skeletal and soft tissue elements within the head) than between functional
54 modules and their underlying genetic components (Conith et al. 2021). Within populations over
55 time, selection also acts on the performance of post-embryonic phenotypes composed of one
56 or more functional modules as organisms interact with their environment (Arnold 1992).Thus,
57 the functional modules observed across species within clades are the product of complex
58 interactions during ontogeny as well as over evolutionary time. Evaluating integration is a
59 means of assessing the strength and pattern of correlation within and between hypothesized
60 modules. Comparative analyses look to patterns of within- and between-module variation
61 across species to test linkages among modularity, phenotypic disparity, functional diversity and
62 the correlated evolution of functional traits (Felice et al. 2018; Watanabe et al. 2018, 2019;
63 Hedrick et al. 2020).
64 Across vertebrates, the sensory systems housed within the cranium (olfactory, visual,
65 and auditory) are often correlated with ecology through diet and foraging (Barton et al. 1995;

66 Thiagavel et al. 2018; Leiser-Miller and Santana 2020). For example, in birds, olfactory bulb size
67 is correlated with behaviors including migratory and foraging strategies (Corfield et al. 2015),
68 and the sizes of visual and olfactory systems are also correlated with activity timing, diet, and
69 habitat in primates, bats, and insectivorous terrestrial mammals (Barton et al. 1995). In addition
70 to their direct roles in foraging and feeding behaviors, these sensory systems are also adjacent
71 to, or sometimes even embedded within, structures that serve mechanical functions. These
72 functions crucially include generating bite force, which determines the types of foods an animal
73 can access and process (Dumont 1999; Aguirre et al. 2002, 2003; Herrel and Holanova 2008;
74 van der Meij and Bout 2008; Santana et al. 2012; Hedrick and Dumont 2018; Deutsch et al.
75 2020).

76 The diversity of cranial phenotypes associated with feeding within noctilionoid bats
77 (Superfamily Noctilionoidea) makes them an ideal system with which to study the relationships
78 between mechanical and sensory regions of the cranium. Noctilionoid bats include 248 species,
79 218 of which comprise the family Phyllostomidae (Fleming et al. 2020), commonly known as the
80 Neotropical leaf-nosed bats. While most phyllostomids exhibit much greater diversity, most
81 noctilionoid families are primarily insectivorous and divergence within lineages presents as
82 subtle changes in body size, foraging style, and echolocation calls (Freeman 2000; Rolfe 2011;
83 Baker et al. 2012; Thiagavel et al. 2018; Rodriguez-Durán and Rosa 2020). Although
84 phyllostomids maintain the ancestral multi-harmonic echolocation calls, they have escaped
85 strict insectivory and diversified into dietary niches that include nectar, fruit, vertebrates, and
86 blood (Fig. 1, also see Fig. 1 in (Dumont et al. 2012)). This great ecological diversity is reflected

87 in the differential reliance of phyllostomid bats on a constellation of sensory and mechanical
88 functions (Teeling et al. 2018; Fleming et al. 2020).
89 In this study we test three broad hypotheses about functionally defined mechanical and
90 sensory modules and their potential influence on ecomorphological diversity across the
91 hyperdiverse clade of noctilionoid bats. First, we hypothesize that mechanical and sensory
92 structures are independent suites of modules. Second, we hypothesize that mechanical and
93 sensory modules have evolved at different rates. Third, we hypothesize that within each
94 module the relationship between phenotypic disparity and rate of evolution differs significantly
95 from a null model in a manner consistent with either evolutionary facilitation (in the case of
96 mechanical modules) or constraint (in the case of sensory modules) (Felice et al. 2018). Given
97 the fundamental link between cranial shape and bite-force in phyllostomids (Dumont et al.
98 2014), we expect higher than expected rates of evolution relative to disparity in mechanical
99 modules (Hu et al. 2016; Arlegi et al. 2018; Hedrick et al. 2020). We further expect that sensory
100 modules are more conserved than mechanical modules because while sensory modules do
101 exhibit phenotypic variation (Hall et al. 2021), ecological diversification has likely resulted in less
102 extensive reorganization of sensory structures. We conclude with a confirmatory test of the
103 association of within-module integration with disparity and rates of module evolution. We also
104 explore the relationship between mechanical and sensory modules at the clade level, among
105 lineages, and with respect to the evolution of shape to gain a more nuanced understanding of
106 their associations.
107
108 **Methods**

109

110 *Taxonomic Sample and 3D Imaging*

111 We sampled 42 individuals from 35 species, covering all families within the neotropical
112 families within Noctilionoidea (Phyllostomidae, Noctilionidae, Mormoopidae, Furipteridae and
113 Thyropteridae) and encompassing a broad range of dietary niches within the clade (Fig 1, S1
114 Table). Some analyses were run on the complete dataset representing all noctilionoids. In other
115 cases, we ran separate analyses for phyllostomids (34 individuals, 28 species), where dietary
116 diversity is concentrated, and for non-phyllostomid noctilionoid families combined (8
117 individuals, 7 species), all of which are insectivorous.

118 To quantify the sizes and shapes of mechanical structures, the olfactory bulb, and
119 cochlea, we visualized the heads of bats using a combination of standard computed
120 tomography (CT) for hard tissues. Bat specimens were scanned using a Nikon Metrology (X-Tek)
121 HMXST225 microCT system at the Center for Nanoscale Systems at Harvard University. Three-
122 dimensional (3D) images were processed following (Hedrick et al. 2020). We generated image
123 stacks using proprietary software associated with the X-Tek scanner (CTPro, Nikon Metrology
124 Inc., Japan), segmented image stacks using Mimics v. 16.0 (Materialise, Leuven, Belgium),
125 created meshes using VGStudio Max 3.0 (Volume Graphics Inc., Germany) and exported them
126 as PLY files.

127 We used reconstructions of eyes previously published by (Hall et al. 2021), which
128 include diffusible iodine-based contrast-enhanced computed tomography (DiceCT; (Gignac et
129 al. 2016; Hedrick and Dumont 2018)) from the same specimens (S1 Table). Briefly, we defined
130 the orbital space surrounding the left eye by its muscular boundaries and eyelid. We used the

volume and location of the orbital space as a proxy for eye location and volume, because it is less subject to distortion than the globe itself in fluid-preserved museum specimens (Hedrick and Dumont 2018).

Placing Landmarks

Our data set included a total of 322 landmarks: 43 fixed landmarks, 160 sliding semi-landmarks on curves, 55 surface landmarks on the eye, and 64 surface landmarks on a patch placed on the palate (S2 Table, S1 & 2 Video) that were placed on 3D meshes using IDAV Landmark Version 3.6 (Wiley et al. 2005). Sliding semi- and surface landmarks are adjusted to reduce their weight in the analysis, thus reducing the potential effect of their representation by large numbers of semi- and surface landmarks. These methods involve sliding neighboring landmarks along curves and surfaces to minimize bending energy and ensure that the arbitrary spacing of semi-landmarks does not influence shape variation (Bookstein 1997; Gunz and Mitteroecker 2013). We placed external landmarks on the external surface of the cranium as per Hedrick et al. (2020). To landmark structures on internal surfaces of the bony skull, 3D models were digitally dissected in Geomagic Studio 2014 (3DSystems, SC, USA) into three parts to reveal the cochlea, the impression left by the olfactory bulb on the internal surface of the skull (anterior cranial fossa), and the internal surface of the cranial base.

We identified landmarks to represent the eye in three steps. First, we used Mimics to calculate the volume and centroid of the orbital space reconstructed by Hall et al (2021). We then generated a sphere of equal volume around the centroid and placed 55 landmarks on its surface. Reducing the eye landmarks to seven (one in the center and six across perpendicular

poles) did not change the results of tests for modularity (S9 Table)), and so we proceeded with the data set of 55 eye landmarks. Because our eye data are based on an idealized and identical shapes, the results of our analyses reflect variation in the orientation and overall size of the eye. Throughout the landmarking process we kept all parts of each specimen in the same coordinate system so that landmarks could be concatenated into a single file using custom R code.

To ensure that the number of landmarks selected did not affect the number of modules recovered, we conducted a sensitivity analysis by down sampling the number of landmarks by 25%, 50% and 75% and testing whether this changed the number of modules detected. Custom code was written in R to subsample within each module systematically; every second landmark (50%), one in every four landmarks (25%), and the first three of every four landmarks (75%). The same number of modules were recovered using EMMLi from the complete set of noctilionoid landmarks and all down-sampled datasets, and vector congruence correlation matrices of the data sets were strongly correlated (R^2 = 0.73 – 0.95; S3 Table). We further tested the effect of landmark number on modularity by regressing the number of landmarks against the ρ coefficient of each module (a measure of integration), first for the whole noctilionoid group and then for the sub-groups of phyllostomids and other noctilionoids. We found no evidence that the number of landmarks in each module influenced modularity (S8 Table). Based on these analyses, we used the full set of 322 landmarks for further analyses. To employ phylogenetic comparative methods and adjust for unequal sample sizes in our analyses, we used species means for taxa represented by multiple individuals (7 species, S1 Table).

Defining Modules

To test hypotheses about modularity of sensory and mechanical systems we grouped landmarks into eight hypothetical modules that encompass anatomical structures associated with specific functions (Fig 1; S1 & 2 Video. Among mammals, the size of sensory structures is often directly related to function. To conserve the size component in our analyses of shape variation, we did not adjust data for allometry. Therefore, our landmark data still carry shape variation that is associated with size. The shapes of some mechanical regions are clearly linked to functional variation (e.g., Dumont 2004; Dumont et al. 2009, 2012; Santana et al. 2012; Neaux et al. 2021). Here we make inferences based on those linkages but do not directly measure mechanical variables. The shapes of sensory structures (e.g., olfactory bulb, cochlear region, and eye) are unlikely to perfectly reflect sensory ability. Likewise, it is likely that some shape changes don't reflect functional change at all (Gould and Lewontin 1979). Nevertheless, we propose that there is at least circumstantial evidence to suggest that each of our eight modules carries some functional signal.

We defined three sensory modules that encompass the olfactory bulb (smell), the cochlea (sound), and the eye (vision) (Figure 1; S1 & 2 Videos). Enlarged eyes are associated with increased visual acuity (Müller and Peichl 2005; Müller et al. 2007; Land and Nilsson 2012; Eklöf et al. 2014; Veilleux and Kirk 2014; Sadier et al. 2018) and eye orientation is related to activity pattern in primates (Heesy 2008). Larger olfactory bulbs support more expansive epithelia and therefore larger surface areas for odor detection (Barton et al. 1995; Buschhüter et al. 2008; Corfield et al. 2015). Enlarged olfactory epithelia are associated with frugivory among noctilionoid bats (Yohe et al. 2021). Finally, cochlear volume and shape is correlated with aspects of cochlear morphology that influence hearing performance (Kössl and Vater 1995;

197 Kirk and Gosselin-Ildari 2009; Vater and Kössl 2011; Davies et al. 2013*a*, 2013*b*). Among bats,
198 variation in the relative volumes of sensory structures often tracks variation in foraging strategy
199 and diet (Barton et al. 1995). For example, the ancestral phyllostomid diverged from its sister
200 taxa in having relatively larger olfactory bulbs and eyes, which is characteristic of frugivory (Hall
201 et al. 2021). Similarly, the shift to plant-based diet in palaeotropical fruit bats (Pteropodidae)
202 allowed larger skulls and brain regions associated with vision, olfaction and spatial memory
203 (Thiagavel et al. 2018). We defined olfactory, cochlear and eye modules with landmarks that
204 encompass the three-dimensional volume as well as shape of those structures (Figure 1, S1 & 2
205 Videos). Olfactory module landmarks were placed on the impression of the olfactory bulb on
206 the internal surface of the skull, cochlea module landmarks were placed on the region of the
207 cranial base that encompasses the cochlea, and the eye module was defined by landmarks
208 placed on the surface of the reconstructed orbital sphere.
209 We defined five mechanical modules that encompass, but do not directly measure,
210 elements of the masticatory system whose shape and size affect bite force and a bat's ability to
211 extract nectar from deep within the corollas of large flowers: the external cranial vault, palate,
212 face, zygomatico-glenoid complex and the cranial base (Figure 1; S1 & 2 Videos). In using these
213 modules, we assume that variation in their shapes reflects, at least in part, known functional
214 variation in their constituent parts. For example, the external cranial vault provides the
215 attachment area of the temporalis muscle, the largest jaw-closing muscle in bats and most
216 other mammals. The temporalis generates the highest jaw-closing moments in bats that
217 consume hard food items (hard fruits, vertebrates) and the lowest jaw-closing in nectar feeding
218 species (Santana et al. 2010, 2012). This variation reflects a combination of differences in the

219 relative muscle size and the shape and orientation of its origin on the external vault relative to
220 the temporomandibular joint (Davis et al. 2010).
221 Likewise, variation in the shape of the palate, and by association the face, is closely
222 associated with the ability to generate bite force. Species with short, broad palates generate
223 relatively higher bite forces for their size than species with long narrow palates (Aguirre et al.
224 2002; Nogueira et al. 2009; Davis et al. 2010; Santana et al. 2010). In mechanical terms, shorter
225 palates (and faces) shorten the out lever when the jaw is modeled as a simple 3rd class lever,
226 thereby increasing mechanical advantage (mechanical advantage = in lever (distance from jaw
227 joint to muscle insertion)/ out lever (distance from bite point to jaw joint, e.g., (Freeman and
228 Lemen 2010). Mechanical advantage has been identified as a target of selection in phyllostomid
229 bats (Dumont et al. 2014) and linked to an increase in speciation rate in fig specialists (Dumont
230 et al. 2012). Palate length is also associated with different loading behaviors during feeding;
231 species with short palates engage in biting behaviors that apply torsional loads to the skull
232 while species with long palates engage in behaviors that apply bending moments (Dumont
233 1999; Dumont et al. 2009; Santana et al. 2012). Finite element analyses further predict that
234 skulls with short, broad palates are more resistant to forces applied under both torsional and
235 bilateral bending loads (Santana et al. 2012; Dumont et al. 2014).
236 While short palates and faces are linked with high bite force, elongated palates and
237 faces support elongated tongues that increase the efficiency of extracting nectar from flowers,
238 and there is evidence for the morphological specialization of nectar-feeding species on flowers
239 with different corolla depths (Paton and Collins 1989; Winter and von Helversen 2003;
240 Gonzalez-Terrazas et al. 2012). The palate and face are often combined into the rostrum. We

keep them separated here, and test the validity of that separation, because it is possible that the shape of the face may vary to accommodate known differences in olfactory bulb and eye volume that has been documented in phyllostomids (Hall et al. 2021), and/or whether echolocation sounds are emitted through the nostrils (phyllostomids) or the mouth (other noctilionoids) (Pedersen 1993, 1998).

The zygomatico-glenoid complex carries two clear functional associations that we assume are reflected in our dataset. The portion of the zygomatic arch we captured in this module reflects the origin of the masseter muscle. Typically, the second largest jaw-closing muscle in mammals, the masseter is the single best predictor of bite force in phyllostomids (Santana et al. 2010) and generates the highest jaw-closing moments in bats that consume soft foods such as soft-bodied insects and soft fruits. The temporomandibular joint is also part of the zygomatico-glenoid module and its location relative to the molar toothrow (and palate) is associated with variation in bat diet (Freeman 1979; Santana et al. 2012). The joint is furthest away from the toothrow in species that exhibit high bite forces driven by large temporalis moments and consume hard foods. Conversely, the jaw joint is closest to the molar toothrow (and palate) in nectar-feeders, which produce very low bite forces and consume primarily liquids.

In bats, the relative position of the cranial base and palate are functionally linked to mode of echolocation (Pedersen 1993) and we assume that relationship is captured in the landmarks that we selected. The angle between the long axes of the cranial base and palate approaches 180° in bats that emit echolocation calls through their mouths (oral-emitters), which aligns the nasopharynx and oral cavity. In contrast, the angle between the cranial base

and palate is more acute in species that emit echolocation calls through their noses (nasal-emitters), creating a clear pathway for sound to travel from the nasopharynx through the nasal cavity and out the nostrils. Phyllostomids are nasal-emitters and other noctilionoids are oral-emitters and so we expect to see differences in the cranial base module between the two groups. The orientation of the cranial base relative to the facial skeleton has also been linked to the ability of the facial skeleton to resist high loads in animals ranging from woodpeckers to primates and at least two extinct mammals (Cartmill 1974; Kenigswald et al. 2005; McCoy and Norris 2012). It is not known if the same is true among bats, but some phyllostomids do consume resistant food items (i.e., seeds (Nogueira et al. 2005)).

Testing Modularity Hypotheses

We tested one null and four functional modularity hypotheses (S4 Table). The null model proposes that eight modules are evolving in tandem as one unit. The first functional hypothesis (M1) addresses our first hypothesis, that all sensory modules are part of one module and all mechanical hypotheses are part of another. Support for this modularity hypothesis would be consistent with the idea that sensory and mechanical systems are each tightly integrated because their parts must be perfectly tuned to function together, but that sensory and mechanical modules are under separate evolutionary pressures. The second functional hypothesis (M2) is that the that the mammalian skull is divided into two functional modules based on development, the neurocranium and the rostrum (face, palate and eye modules combined). This hypothesis is supported by many studies and implies that either the rostrum, the neurocranium or the relationship between them is the locus of shape changes that affect

functional diversity (e.g., (Marroig et al. 2009; Porto et al. 2009; Santana and Lofgren 2013; Hedrick et al. 2020)). The third functional hypothesis (M3) is that the face and palate constitute a single module and all other modules are separate and independent of one another. This hypothesis addresses the fact that dietary differentiation among phyllostomids is primarily driven by rostral elongation and shortening (Freeman 2000; Dumont et al. 2012; Hedrick et al. 2020). The fourth functional hypothesis (M4) proposes that all eight modules are independent and therefore, to varying extents, free to interact with one another.

We tested the relative strength of these five modularity hypotheses using the EMMLi package in R (Goswami and Finarelli 2016), which uses a maximum likelihood approach to compare sets of modularity hypotheses and applies the Akaike Information Criterion corrected for small sample sizes (AICc). We implemented EMMLi for the dataset encompassing all noctilionoids, and again after partitioning it into phyllostomids and non-phyllostomid noctilionoids. We quantified effect sizes using the modularity.test function from the Geomorph package in R (Adams and Collyer 2019) to evaluate whether modularity differed significantly between the three partitions

We also indirectly tested the independence of the resulting modules by comparing their rates of shape change using Bayestraits (see *Visualizing Module Evolution*). These and all other evolutionary analyses were based on the time-calibrated phylogeny of (Rojas et al. 2016) pruned to reflect our sample (Fig 1). First, we calculated the net rate of shape evolution of each module across all noctilionoids using *geomorph* in R with 1000 random permutations and a Brownian Motion (BM) model of evolution (Adams and Otárola-Castillo 2013). We then tested whether these rates were significantly different across the modules and between phyllostomids

and other noctilionoids using function 'compare.multi.evol.rates' in *geomorph* (Denton and Adams 2015), which compares net rates of morphological evolution for multi-dimensional traits under a Brownian motion model of evolution.

Visualizing Module Evolution

We visualized the evolution of each module across all noctilionoids in three ways to evaluate patterns of change at three hierarchical scales: normalized average rates of evolution through time, relative rates of evolution among lineages, and rates and directions of module shape changes.

We plotted rates of evolution for each module across evolutionary time using BayesTraits (Meade and Pagel 2016) and the R package BTR tools (Ferguson-Gow 2017) as in Felice et al (2018). This rate through time plot illustrates the average rate of each module's evolution *across* lineages within successive time bins relative to that module's maximum average evolutionary rate and provides an overview of rate changes within modules over time relative to one another. BayesTraits detects lineage diversification and multivariate trait evolution using reverse-jump MCMCs. Principal component analyses of the Procrustes coordinates for each module were used to generate trait (shape) data for each module. The input data were principal components accounting for the first 95% of total variance and the time-calibrated phylogeny (Rojas et al. 2016). Using a variable rates model with the independent contrasts and autotune options, we ran 110 million iterations and discarded the first ten million as burn-in. BayesTraits also evaluates five evolutionary models (BM, Lambda (λ), Delta (δ), Kappa (κ), and a single peak OU model) and the best supported model is identified

using Bayes factors (Meade and Pagel 2016). We plotted the rate through time using one-million-year time bins from the best rate model for each module using BTR tools package in R. The average rate across branches for each time bin was corrected by the maximum average rate attained for that module according to (Felice et al. 2018). We noted the timing of seven events associated with positively selected visual genes and dietary changes within the plot (Davies et al. 2020): the last common ancestor of the Noctilionoidea, Mormoopidae, Phyllostomidae, all plant feeding phyllostomids, nectar-feeding Glossophaginae and Lonchophyllinae, and fig-eating Stenodermatinae.

We also visualized by illustrating the rate of evolution of each module across the noctilionoid phylogeny. We created a 'rate tree' for each module using the best supported evolutionary model in BayesTraits and then scaled each tree by its maximum rate. Visual comparison of rate trees among modules can reveal lineage-specific patterns of correlated increases or decreases in evolutionary rates that are obscured in the rate through time plot. It can also reveal the extent to which the rate through time plot may be influenced by the concentration of fast rates in a small number of lineages.

Finally, we visualized the evolution of modules by plotting shape (i.e., principal components of shape) across the phylogeny for each module. These plots illustrate not only the rate and timing of shape change, but also its direction. Module shape is associated with module function and so qualitative comparisons of character states among modules can provide insights into how mechanical and sensory functions may, and may not, have changed in concert during noctilionoid evolution. We plotted the first and second principal components of shape (PC1 and PC2) where most of the variation was concentrated (63 – 93 % - 1^{st} + 2^{nd} PC;

Base = 63%, Olfactory Bulb = 71%, Cochlea Region = 72%, Palate = 76%, Face = 78%, External Vault = 85%, Eye = 88%, Zygo-glenoid complex = 93%).

Evaluating Disparity and Integration

We tested the hypothesis that within each module the relationship between phenotypic disparity and rate of shape evolution differs significantly from a null, Brownian model, in a way that is consistent with either evolutionary facilitation or constraint. Average disparity for each module (Procrustes variance) was calculated from Procrustes distances of all the landmarks within the module. The average rate of evolution of each module (sigma) was calculated as the average of the sum of sigma values of each of the coordinates (x, y, and z) within that module (Revell et al. 2008; Adams and Otárola-Castillo 2013). Procrustes variance within each module was then plotted against the evolutionary rate (sigma) for each landmark with the BM expectation of evolution of uncorrelated traits. We used standardized major axis regressions to compare each module's regression against the slope predicted under a BM model using R package *smatr* (Warton et al. 2012; Felice et al. 2018). Each module's slope was also compared against that of other modules.

To explore whether integration influences the disparity and evolutionary rate of module shape across all noctilionoids, we regressed the average rate of evolution (sigma), average disparity (Procrustes variance) and average integration of each module (ρ coefficient) against each other. The ρ coefficient was derived from the EMMLi analysis.

Results

We found significant support for all eight mechanical and sensory modules within Noctilionoidea as a whole, as well as within phyllostomids and among all non-phyllostomid noctilionoids (S5 Table). All other hypotheses of modularity were rejected. The whole noctilionoid group (Zcr -13.5993 ± SE 0.0110, p = 0.002), only phyllostomids (Zcr = -13.1809 ± SE 0.107, p = 0.004), and other noctilionoid species (Zcr = -10.74024 ± SE 0.0108, p = 0.004) all exhibited significant modularity.

Noctilionoids as a whole exhibited high within-module integration of the eye, zygomatico-glenoid complex and face (diagonal values, Fig. 2). In general, between-module integration is of intermediate strength and evenly distributed, with similar levels of integration between and among sensory and mechanical modules (off-diagonal values in Fig. 2). There is low integration between the eye and cranial base, and between the olfactory bulb and both the cochlea and zygomatico-glenoid complex. In contrast, the integration between the zygomatico-glenoid complex and the eye, external vault, palate, and face is relatively high. Noctilionoidea as a group exhibits stronger integration among mechanical modules, among sensory modules, and between mechanical-sensory modules than both phyllostomids and non-phyllostomid noctilionoids.

The relatively uniform and strong integration within and between modules in Noctilionoidea masks distinct differences in within- and between-module integration (diagonal and off-diagonal values, respectively) between phyllostomids and non-phyllostomid noctilionoids. Within-module integration of the eye, zygomatico-glenoid complex and face is strong within the two subgroups, echoing the pattern across Noctilionoidea (diagonal values, Fig. 2). Among sensory modules, phyllostomids exhibit higher within-module integration of the

olfactory bulb and, to a lesser extent, the cochlea. With respect to mechanical modules, phyllostomids exhibit higher integration of the external vault, while non-phyllostomid noctilionoids exhibit higher within-module integration of the zygomatico-glenoid complex, face and palate. The integration of the cranial base is similar across all three data sets.

With respect to between-module integration, phyllostomids exhibit weaker relationships among mechanical modules and stronger relationships between sensory (eye and olfactory bulb) and mechanical modules than do non-phyllostomid noctilionoids (off-diagonal values, Fig. 2). In phyllostomids the integration of the eye and olfactory bulb is weaker, while the integration of the eye and the cochlea is stronger than in non-phyllostomid noctilionoids. In contrast to phyllostomids, integration of mechanical modules is much higher among non-phyllostomid noctilionoids. The olfactory bulb is more strongly integrated with mechanical modules among phyllostomids, as is the integration of the eye with the palate, face and zygomatico-glenoid complex. In contrast, the cochlea is more strongly integrated with most mechanical modules in non-phyllostomid noctilionoids. The exception is the external vault, which is more closely tied to the cochlea in phyllostomids. Overall, the average strength of integration among sensory module and mechanical module subsets is similar within phyllostomids and non-phyllostomid noctilionoids (mean $\rho = 0.31$ and 0.30), while mechanical modules are almost twice as integrated as sensory modules among non-phyllostomid noctilionoids than in phyllostomids (mean: $\rho = 0.46$ and $\rho = 0.25$).

In support of the hypothesis that modules evolved at different rates, we found substantial heterogeneity in net rates of evolution among sensory and mechanical modules for all noctilionoids, within phyllostomids, and within non-phyllostomid noctilionoids (S6 Table). On

417 average, phyllostomids have a higher mean rate of module evolution (7.62E-07 ± 1.90E-07
418 σ^2mult) than non-phyllostomid noctilionoids (5.13E-07 ± 1.43E-07 σ^2mult). The fastest evolving
419 module in both groups is the external cranial vault, followed by the face in phyllostomids and
420 the zygomatico-glenoid complex in non-phyllostomid noctilionoids. The slowest evolving
421 module in both phyllostomids and non-phyllostomid noctilionoids is the eye, followed by the
422 cochlea in non-phyllostomid noctilionoids and the palate in phyllostomids. There are a few
423 differences in mean rates of evolution between mechanical modules within phyllostomids and
424 within non-phyllostomid noctilionoids, but no significant differences among sensory modules.
425 The rate of evolution of the external cranial vault is significantly higher than the palate in both
426 groups, and the rate of evolution of the face is significantly higher than that of the palate in
427 non-phyllostomid noctilionoids. Looking across sensory and mechanical modules, several
428 mechanical modules evolve significantly faster than the eye: the external cranial vault and face
429 modules in both subgroups, and the zygomatico-glenoid complex in phyllostomids.
430 Figure 3 illustrates the relative rate of evolution for each module through time. The
431 most striking pattern is that rates of evolution of sensory modules tend to peak earlier than
432 those of mechanical modules. Among sensory modules, early increases in the evolutionary
433 rates of the eye and cochlea modules preceded those of the olfactory module, which
434 subsequently increased just before the emergence of the Mormoopidae. All three sensory
435 modules attained peak rates before the divergence of the phyllostomids and have gradually
436 slowed since. Mechanical modules also exhibit rate increases immediately preceding the
437 divergence of the phyllostomids but only the zygomatico-glenoid complex and the face
438 modules reach their peak rates at this time. Following the origin of phyllostomids, there is much

more disparity in rates of mechanical module evolution, and the peak rates for the palate, external vault, and skull base modules are very close to the present. The short-face stenodermatines and the long-faced glossophagines represent the two extremes of cranial morphology among phyllostomids, and there are concerted decreases in the rates of evolution of the face, zygomatico-glenoid and external cranial vault occurring just prior to the origin of both clades. The rate of evolution of the palate module increases just before the appearance of the stenodermatine ancestor. Overall, the rates of sensory module evolution peak before the origin of phyllostomids and then decline steadily over time. In contrast, rates of mechanical module evolution peak either before the origins of phyllostomids or very recently and are far more variable throughout the evolution of noctilionoids.

Figure 4 shows relative rates of module evolution across the phylogeny and showcases rate heterogeneity among lineages. While Figure 3 illustrates that peak mean evolutionary rates of sensory modules preceded those of mechanical modules when all species are combined, Figure 4 illustrates influence of individual taxa in driving that pattern. For example, some of the highest rates of sensory module evolution occur in the earliest lineages. Comparing rates of module evolution reveals several instances of parallel rate shifts that suggest correlated change. The eye is the sensory module with the most evenly distributed rates across the phylogeny and its rapid evolution at the base of phyllostomids is accompanied by modest rate changes in all mechanical modules. Similarly, rates of olfactory bulb evolution are low along the backbone of the tree but exhibit a small increase at the base of the fig-feeding stenodermatines, perhaps in concert with rate increases in in the eye, palate, cranial base, and external cranial vault module. There are marked increases in the evolutionary rate of the eye

and face modules in the branch leading to the hairy big-eyed bat, *Chiroderma villosum*. Among mechanical modules, there are correlated increases in the rates of face and palate module evolution in lineages ancestral to nectar-feeders. Patterns of rate change are similar among the zygomatico-glenoid complex, external vault, and cranial base, with the latter two exhibiting high rates of evolution in the lineage ancestral to the Jamaican fruit bat, *Artibeus jamaicensis*.

By illustrating the rate and direction of changes in shape (principal components of shape) for each module across the phylogeny, Figure 5 and Supplementary Figures 2–7 offer the most nuanced picture of module evolution. While shape as represented by PC1 separates phyllostomids from non-phyllostomid noctilionoids, PC2 separates taxa according to dietary guild and lineage. In most cases nectarivores are clearly distinguished from their sister taxa along PC2, with high values for some modules (cochlea, eye, cranial base, zygomatico-glenoid and palate) and low values for others (external vault and face). Nectarivores and phyllostomid generalists share low PC2 values for the olfactory bulb (Figure 5). PC2 values for the fig-feeding sternodermatines as a group are less distinct than those of nectar-feeders. Instead, extreme PC2 values are common in the most short-faced species (*Phyllops falcatus* and *Centurio senex*) and, for the face and olfactory bulb modules, the big-eyed bat *Chiroderma villosum*. The morphologically intermediate non-phyllostomid noctilionoids exhibit intermediate PC2 values for most modules.

Our third hypothesis was that the relationship between phenotypic disparity and rate of evolution within each module departs from the Brownian model indicating constraint or selection (Felice et al. 2018) and that this relationship varies among modules. We expected sensory modules to have significantly lower slopes than the null model, indicative of constraint,

and mechanical modules to have significantly higher slopes, suggesting that modularity facilitated diversification of trait values, especially among phyllostomids. Consistent with this expectation, we found significantly lower than predicted slopes for all three sensory modules within phyllostomids (Table 1). The slope for the eye was also lower than predicted among non-phyllostomid noctilionoids, but the slope of the olfactory bulb was significantly higher. Among the mechanical modules, two were significantly lower among phyllostomids (base and external vault), while three of the five were significantly higher in non-phyllostomid noctilionoids (external vault, palate, and face). Overall, we did find evidence for evolutionary constraint and selection, but not always in the ways we predicted (see discussion).

493 **Table 1:** Results from major axis regression comparing the observed variance - rate relationships to the relationship predicted under
494 Brownian motion evolution of uncorrelated traits. Type indicates the Brownian Motion null (BM), sensory modules (S) and mechanical
495 modules (M). Results with p-values < 0.05 indicating significant deviation from the slope of the null model are bold.

496

		All neotropical noctilionoids				**Phyllostomids**				**Other noctilionoids**			
Type	**Module**	**Slope**	**lower**	**upper**	**p value**	**Slope**	**lower**	**upper**	**p value**	**Slope**	**lower**	**upper**	**p value**
BM		0.30	0.30	0.32		0.26	0.25	0.27		0.31	0.29	0.33	
S	Eye	0.39	0.30	0.49	0.0582	**0.13**	0.11	0.16	6.88E-11	**0.16**	0.14	0.18	1.21E-08
S	Olfactory Bulb	**0.14**	0.11	0.18	5.64E-09	**0.06**	0.04	0.07	2.22E-16	**0.52**	0.44	0.61	6.88E-11
S	Cochlea	**0.16**	0.13	0.18	6.40E-13	**0.07**	0.06	0.09	2.22E-16	0.26	0.24	0.29	0.8319
M	Base	**0.12**	0.09	0.17	2.32E-06	**0.09**	0.06	0.12	7.31E-07	0.37	0.26	0.53	0.0680
M	External Vault	0.32	0.25	0.40	0.6659	**-0.13**	-0.19	-0.08	0.0018	**0.55**	0.52	0.59	2.22E-16
M	Palate	**0.37**	0.33	0.40	0.0002	0.24	0.22	0.27	0.3274	**0.65**	0.59	0.73	2.22E-16
M	Zygomatico-glenoid	0.22	0.05	0.92	0.5320	0.09	0.02	0.55	0.2071	0.38	0.16	0.89	0.2356
M	Face	0.38	0.30	0.47	0.0572	0.31	0.26	0.37	0.09	**0.34**	0.29	0.41	0.0036

497

Finally, to assess their potential effects on one another, we explored the relationship between integration and disparity and between integration and evolutionary rate across all noctilionoids (Fig. 6). Across modules, disparity increases with increasing evolutionary rate (R = 0.63, $p < 0.01$), and the zygomatico-glenoid complex and external vault are the fastest-evolving and most disparate. Within modules, there is no evidence of a relationship between integration and either the rate of module evolution (R = -0.14, p = 0.91) or the module disparity (R = -0.13, p = 0.86).

Discussion

By investigating two sets of functional modules whose relationships are largely unexplored – sensory modules that receive cues crucial to foraging, and mechanical modules that contribute to bite force – we identified patterns of evolutionary changes in modules related to food perception and processing. We found no support for the hypothesis that sensory and mechanical modules are two independent suites of modules. Instead, we found eight independent functional modules with varying rates of evolution, which could have provided noctilionoids with a complex and rich stage on which selection could act (Table S4 & 5). Our data also supports the hypothesis that disparity emerges from differential rates of evolution across mechanical and sensory modules (Fig 3 & Table S6) and not from variation in modularity itself (Fig 6). This study extends beyond documenting mosaic evolution in the head (e.g.,(Rossoni et al. 2019)) to identify differential evolutionary rates as the underlying mechanism. The integration of some sensory and mechanical modules (Figure 2), as well as

some coordinated rate changes (Figure 3 & 4), may imply that the two systems have evolved synergistically, thereby linking abilities to sense and process novel foods. For example, phyllostomids are characterized by a newly evolved linkage between mechanical modules and the olfactory bulb and eye, and a release from the association between mechanical modules and the cochlea (Fig 2). From a functional perspective, the coupling of mechanical modules with the visual and olfactory systems is consistent with a fundamental shift to foraging for plants, which relies more heavily on vision and olfaction than does aerial insectivory. The timing of this change at the clade level (Fig 3 & 4) indicates that a shift in the evolution of sensory modules that predated most changes in mechanical modules, supporting a sensory-first hypothesis of diversification. We propose that shifts in evolutionary rates could have affected integration among modules, opened new dietary niches and provided the structural flexibility that was necessary for the radiation of noctilionoid bats. Perhaps the same scenario played out in other vertebrate clades.

Our work explores the interplay of sensory and mechanical functions within an ecomorphologically diverse radiation, providing a more holistic perspective on functional ecology than analyses of integration based on hypothesized developmental modules (Hedrick et al. 2020), or analyses that focus solely on mechanical modules (Monteiro and Nogueira 2010). We found that the strength of integration within mechanical and sensory modules is similar and relatively low within phyllostomids. In contrast, the strength of integration within mechanical modules is high and nearly twice as strong as integration within sensory modules among non-phyllostomid noctilionoids. In contrast to Hedrick et al.'s (2020) analysis of a developmental, two-module model (rostrum and basicranium/cranium), which concluded that

542 phyllostomids are twice as integrated and less disparate than non-phyllostomid noctilionoids,
543 we found that phyllostomids are less integrated when considering eight, finer-scale partitions
544 of the cranium into mechanical and sensory modules (higher Zcr than other noctilionoids (ref:
545 results section 1st paragraph). We propose that considering finer scale, functional modules and
546 their relationships to one another offers more detailed insight into the context for
547 diversification than developmental modules provide.
548 Visualizing module evolution at three hierarchical scales provided increasingly detailed
549 insight into how module shapes changed relative to one another over time. The rate through
550 time plot (Fig. 3) provided a clade-level snapshot of the mosaic evolution of modules across
551 Noctilionoidea. Rate trees for each module further revealed that rates of module evolution
552 were, on balance, faster in lineages that predate the origin of phyllostomids (Fig. 4). Analyses of
553 character state evolution provide the clearest picture of correlated structural change (Fig. 5,
554 Sup. Figs. 1-6). Shape changes along PC1 separate phyllostomids from other noctilionoids,
555 whereas PC2 (primarily shape and orientation) separated dietary guilds among phyllostomids,
556 especially nectarivores. We propose that major changes early in the evolution of noctilionoids
557 resulted in differences in evolvability between phyllostomids and their sister taxa. The
558 subsequent radiation of phyllostomids did not require major reorganization of modules.
559 Among phyllostomids, parallel changes in sensory and mechanical abilities, such as the
560 ability to both detect and process hard and ripe fruits, may have enhanced access to food
561 (Davies et al. 2013*b*, 2013*a*, 2020; Thiagavel et al. 2018). This is suggested by the small, parallel
562 clade-level rate shifts in the olfactory, eye, face and cranial base modules just before the origin
563 of stenodermatines (Fig. 3), which is reinforced by correlated rate shifts in olfactory, eye,

palate, cranial base, and external cranial vault modules along the lineage leading to stenodermatines (Fig. 4). Stenodermatine bats have short, broad faces and stout crania, which allows the expansion of the olfactory bulb (Fig. 5) as well as enlarged eyes and more robust zygomatic arches. In contrast, the nectar feeding lineages have elevated rates of evolution in the palate, face, and to an extent skull base and eye modules (Fig. 4). These changes resulted in their elongated, narrow skulls and palates, which are associated with reaching into the corollas of flowers, and the repositioning of the eye (Sup. Fig. 1). By identifying multiple functional modules and their interrelationships, our work demonstrates how parallel changes in sensory and mechanical modules were associated with the ecomorphological diversification of phyllostomids. Our results align with the predictions that preadaptation in sensory systems played a leading role in the evolution of bats (Thiagavel et al. 2018; Davies et al. 2020) and that the earliest phyllostomids experimented with foods beyond insects (Freeman 2000; Baker et al. 2012; Hedrick et al. 2020). We added context to these predictions by illustrating that changes in the rates of sensory module evolution occurred in concert with changes in the evolutionary rates of some mechanical modules including the face, zygomatico-glenoid complex, palate and external vault, just before the appearance of the phyllostomid ancestor (Fig 3). Phyllostomids are characterized by a thicker olfactory bulb that occupies relatively more space, and alignment of the palate and cranial base (Fig 5). These changes are consistent with a plant/fruit-based diet requiring higher odor acuity (Barton et al. 1995; Buschhüter et al. 2008; Corfield et al. 2015) and the shift from oral to nasal emission of echolocation sounds (Pedersen, 1993).

Rather than arising from ecological opportunity alone, we propose that intrinsic changes in morphological structure —modularity, integration, and the rates of evolution among

586 mechanical and sensory modules — also contribute to the explosive ecological and phenotypic
587 radiation of phyllostomids. Exposed to similar ecological conditions in the Neotropics, none of
588 the other 6 families of bats exhibit similar levels of phenotypic disparity or species diversity. The
589 ancestor of phyllostomids was distinguished by simultaneous changes in the evolutionary rates
590 of the zygomatico-glenoid complex, face, olfactory bulb, and cochlea that are not associated
591 with changes in the degree of within-module integration (Fig 6). Instead, phenotypic
592 innovation emerged through variable rates of module shape evolution, which allowed different
593 combinations of sensory and mechanical functions over time. Coordination of corresponding
594 functions, such as changes in bite force, olfaction, and echolocation, provided the phyllostomid
595 ancestor with the ability to diversify into available plant-based niches. As a result, we propose
596 that the explosive phyllostomid radiation was facilitated by structural opportunity in addition to
597 ecological opportunity. Ecology alone cannot explain taxonomic radiation: the underlying
598 morphological structures, correlations among those structures, and their functions shape the
599 nature of an organism's relationship with its environment.
600
601
602

References:

Adams, D. C., and M. L. Collyer. 2019. Comparing the strength of modular signal, and evaluating alternative modular hypotheses, using covariance ratio effect sizes with morphometric data. Evolution 1902511:2352–2367.

Adams, D. C., and E. Otárola-Castillo. 2013. Geomorph: An r package for the collection and analysis of geometric morphometric shape data. Methods in Ecology and Evolution 4:393–399.

Aguirre, L. F., A. Herrel, R. van Damme, and E. Matthysen. 2002. Ecomorphological analysis of trophic niche partitioning in a tropical savannah bat community. Proceedings of the Royal Society of London. Series B: Biological Sciences 269:1271–8.

Aguirre, L. F., A. Herrel, R. Van Damme, and E. Matthysen. 2003. The implications of food hardness for diet in bats. Functional Ecology 17:201–212.

Arlegi, M., A. Gómez-Robles, and A. Gómez-Olivencia. 2018. Morphological integration in the gorilla, chimpanzee, and human neck. American Journal of Physical Anthropology 166:408–416.

Arnold, S. J. 1992. Constraints on phenotypic evolution. The American Naturalist 140:S85–S107.

Assis, A. P. A., B. M. A. Costa, D. M. Rossoni, D. Melo, and G. Marroig. 2016. Modularity and Integration. Encyclopedia of Evolutionary Biology 34–40.

Atchley, W. R., and B. K. Hall. 1991. A model for development and evolution of complex morphological structures. Biological Reviews of the Cambridge Philosophical Society 66:101–157.

Baker, R. J., O. R. P. Bininda-Emonds, H. Mantilla-Meluk, C. A. Porter, and R. A. Van Den Bussche. 2012. Molecular time scale of diversification of feeding strategy and morphology in

624 New World Leaf-Nosed Bats (Phyllostomidae): A phylogenetic perspective. Evolutionary History
625 of Bats: Fossils, Molecules and Morphology 385–409.
626 Bardua, C., M. Wilkinson, D. J. Gower, E. Sherratt, and A. Goswami. 2019. Morphological
627 evolution and modularity of the caecilian skull. BMC Evolutionary Biology 19:1–23.
628 Barton, R. A., A. Purvis, and P. H. Harvey. 1995. Evolutionary radiation of visual and olfactory
629 brain systems in primates, bats and insectivores. Philosophical Transactions of the Royal Society
630 of London. Series B: Biological Sciences 348:381–392.
631 Bookstein, F. L. 1997. Landmark methods for forms without landmarks: morphometrics of
632 group differences in outline shape. Medical Image Analysis 1:225–243.
633 Buschhüter, D., M. Smitka, S. Puschmann, J. C. Gerber, M. Witt, N. D. Abolmaali, and T.
634 Hummel. 2008. Correlation between olfactory bulb volume and olfactory function. Neuroimage
635 42:498–502.
636 Camilieri-Asch, V., J. A. Shaw, A. Mehnert, K. E. Yopak, J. C. Partridge, and S. P. Collin. 2020.
637 diceCT: A Valuable Technique to Study the Nervous System of Fish. Eneuro 7.
638 Cartmill, M. 1974. Daubentonia, Dactylopsila, woodpeckers and klinorhynchy. Prosimian biology
639 655–670.
640 Clune, J., J.-B. Mouret, and H. Lipson. 2013. The evolutionary origins of modularity. Proceedings
641 of the Royal Society b: Biological sciences 280.
642 Conith, A. J., S. A. Hope, B. H. Chhouk, and R. C. Albertson. 2021. Weak genetic signal for
643 phenotypic integration implicates developmental processes as major regulators of trait
644 covariation. Mollecular Ecology 30:464–480.

645 Conith, A. J., D. T. Lam, and R. C. Albertson. 2019. Muscle-induced loading as an important
646 source of variation in craniofacial skeletal shape. Genesis 57:1–13.
647 Corfield, J. R., K. Price, A. N. Iwaniuk, C. Gutiérrez-Ibáñez, T. Birkhead, and D. R. Wylie. 2015.
648 Diversity in olfactory bulb size in birds reflects allometry, ecology, and phylogeny. Frontiers in
649 Neuroanatomy 9:102.
650 Davies, K. T. J., P. J. J. Bates, I. Maryanto, J. A. Cotton, and S. J. Rossiter. 2013*a*. The Evolution of
651 Bat Vestibular Systems in the Face of Potential Antagonistic Selection Pressures for Flight and
652 Echolocation. PLoS ONE 8:8–10.
653 Davies, K. T. J., I. Maryanto, and S. J. Rossiter. 2013*b*. Evolutionary origins of ultrasonic hearing
654 and laryngeal echolocation in bats inferred from morphological analyses of the inner ear.
655 Frontiers in Zoology 10:1–15.
656 Davies, K. T. J., L. R. Yohe, J. Almonte, M. K. R. Sánchez, E. M. Rengifo, E. R. Dumont, K. E. Sears,
657 et al. 2020. Foraging shifts and visual preadaptation in ecologically diverse bats. Molecular
658 Ecology 29:1839–1859.
659 Davis, J. L., S. E. Santana, E. R. Dumont, and I. R. Grosse. 2010. Predicting bite force in
660 mammals: two-dimensional versus three-dimensional lever models. Journal of Experimental
661 Biology 213:1844–1851.
662 Denton, J. S. S., and D. C. Adams. 2015. A new phylogenetic test for comparing multiple high-
663 dimensional evolutionary rates suggests interplay of evolutionary rates and modularity in
664 lanternfishes (Myctophiformes; Myctophidae). Evolution 69:2425–2440.

665 Deutsch, A. R., E. Dickinson, K. C. Leonard, F. Pastor, M. N. Muchlinski, and A. Hartstone-Rose.
666 2020. Scaling of anatomically derived maximal bite force in primates. The Anatomical Record
667 303:2026–2035.
668 Dumont, E. R. 1999. The effect of food hardness on feeding behaviour in frugivorous bats
669 (Phyllostomidae): an experimental study. Journal of Zoology 248:219–229.
670 Dumont, E. R. 2004. Patterns of diversity in cranial shape among plant-visiting bats. Acta
671 Chiropterologica 6:59–74.
672 Dumont, E. R., L. M. Dávalos, A. Goldberg, S. E. Santana, K. Rex, C. C. Voigt, E. R. Dumont, et al.
673 2012. Morphological innovation , diversification and invasion of a new adaptive zone.
674 Proceedings of the Royal Society B: Biological Sciences 279:1797-1805.
675 Dumont, E. R., A. Herrel, R. A. Medellín, J. A. Vargas-Contreras, and S. E. Santana. 2009. Built to
676 bite: Cranial design and function in the wrinkle-faced bat. Journal of Zoology 279:329–337.
677 Dumont, E. R., K. Samadevam, I. Grosse, O. M. Warsi, B. Baird, and L. M. Davalos. 2014.
678 Selection for mechanical advantage underlies multiple cranial optima in new world leaf-nosed
679 bats. Evolution 68:1436–1449.
680 Eklöf, J., J. Šuba, G. Petersons, and J. Rydell. 2014. Visual acuity and eye size in five European
681 bat species in relation to foraging and migration strategies. Environmental and Experimental
682 Biology 12:1–6.
683 Esteve-altava, B. 2017. In search of morphological modules : a systematic review. Biological
684 Reviews 92:1332–1347.

685 Evans, K. M., B. Waltz, V. Tagliacollo, P. Chakrabarty, and J. S. Albert. 2017. Why the short face?
686 Developmental disintegration of the neurocranium drives convergent evolution in neotropical
687 electric fishes. Ecology and Evolution 7:1783–1801.
688 Felice, R. N., and A. Goswami. 2017. Developmental origins of mosaic evolution in the avian
689 cranium _Supplementary. Proceedings of the National Academy of Sciences 115:555–560.
690 Felice, R. N., M. Randau, and A. Goswami. 2018. A fly in a tube: Macroevolutionary expectations
691 for integrated phenotypes. Evolution 2580–2594.
692 Ferguson-Gow, H. 2017. BTRTools: A set of tools for processing and analysing the output of
693 BayesTraits. Github.
694 Fleming, T. H., L. M. Dávalos, and M. A. R. Mello. 2020. Phyllostomid Bats: A Unique Mammalian
695 Radiation. University of Chicago Press.
696 Freeman, P. W. 1979. Specialized insectivory: beetle-eating and moth-eating molossid bats.
697 Journal of Mammalogy 60:467–479.
698 Freeman, P. W. 2000. Macroevolution in Microchiropteria: Recoupling morphology and ecology
699 with phylogeny. Evolutionary Ecology Research 2:317–335.
700 Freeman, P. W., and C. A. Lemen. 2010. Simple predictors of bite force in bats: the good, the
701 better and the better still. Journal of Zoology 282:284–290.
702 Gignac, P. M., N. J. Kley, J. A. Clarke, M. W. Colbert, A. C. Morhardt, D. Cerio, I. N. Cost, et al.
703 2016. Diffusible iodine-based contrast-enhanced computed tomography (diceCT): an emerging
704 tool for rapid, high-resolution, 3-D imaging of metazoan soft tissues. Journal of Anatomy
705 228:889–909.

706 Gonzalez-Terrazas, T. P., R. A. Medellin, M. Knörnschild, and M. Tschapka. 2012. Morphological
707 specialization influences nectar extraction efficiency of sympatric nectar-feeding bats. Journal
708 of Experimental Biology 215:3989–3996.
709 Goswami, A. 2006. Cranial Modularity Shifts during Mammalian Evolution. The American
710 Naturalist 168:270–280.
711 Goswami, A., and J. A. Finarelli. 2016. EMMLi: a maximum likelihood approach to the analysis of
712 modularity. Evolution 70:1622–1637.
713 Goswami, A., and P. D. Polly. 2010. The influence of modularity on cranial morphological
714 disparity in carnivora and primates (mammalia). PLoS ONE 5:1–8.
715 Goswami, A., J. B. Smaers, C. Soligo, and P. D. Polly. 2014. The macroevolutionary consequences
716 of phenotypic integration: from development to deep time. Philosophical Transactions of the
717 Royal Society B: Biological Sciences 369:20130254.
718 Gould, S. J., and R. T. Lewontin. 1979. The spandrels of San Marco and the Panglossian
719 paradigm. Proc. R. Soc, Lond. B 205:581–598.
720 Gunz, P., and P. Mitteroecker. 2013. Semilandmarks: a method for quantifying curves and
721 surfaces. Hystrix, the Italian journal of mammalogy 24:103–109.
722 Hall, R. P., G. L. Mutumi, B. P. Hedrick, L. R. Yohe, A. Sadier, K. T. J. Davies, L. M. Dávalos, et al.
723 2021. Find the Food First: An Omnivorous Sensory Morphotype Predates Biomechanical
724 Specialization for Plant Based Diets in Phyllostomid Bats. Evolution.
725 Hedrick, B. P. B. P., G. L. G. L. Mutumi, V. D. D. Munteanu, A. Sadier, K. T. J. K. T. J. Davies, S. J. S.
726 J. Rossiter, K. E. K. E. Sears, et al. 2020. Morphological Diversification under High Integration in a
727 Hyper Diverse Mammal Clade. Journal of Mammalian Evolution 27:1–13.

728 Hedrick, B. P., and E. R. Dumont. 2018. Putting the leaf-nosed bats in context: A geometric
729 morphometric analysis of three of the largest families of bats. Journal of Mammalogy 99:1042–
730 1054.
731 Heesy, C. P. 2008. Ecomorphology of orbit orientation and the adaptive significance of binocular
732 vision in primates and other mammals. Brain, Behavior and Evolution 71:54–67.
733 Herrel, A., and V. Holanova. 2008. Cranial morphology and bite force in Chamaeleolis lizards--
734 adaptations to molluscivory? Zoology 111:467–475.
735 Hu, Y., L. Ghigliotti, M. Vacchi, E. Pisano, H. W. Detrich, and R. C. Albertson. 2016. Evolution in
736 an extreme environment: Developmental biases and phenotypic integration in the adaptive
737 radiation of antarctic notothenioids. BMC Evolutionary Biology 16:1–13.
738 Kenigswald, W. V., K. D. Rose, L. Grande, and R. D. Martin. 2005. First apatemyid skeleton from
739 the lower Eocene Fossil Butte Member, Wyoming (USA), compared to the European apatemyid
740 from Messel, Germany. Palaeontographica, Abteilung A: Palaozoologie-Stratigraphie 272:149–
741 169.
742 Kirk, E. C., and A. D. Gosselin-Ildari. 2009. Cochlear labyrinth volume and hearing abilities in
743 primates. The Anatomical Record: Advances in Integrative Anatomy and Evolutionary Biology
744 292:765–776.
745 Klingenberg, C. P. 2010. Evolution and development of shape: integrating quantitative
746 approaches. Nature Reviews Genetics 11:623–635.
747 Klingenberg, C. P., L. J. Leamy, and J. M. Cheverud. 2004. Integration and modularity of
748 quantitative trait locus effects on geometric shape in the mouse mandible. Genetics 166:1909–
749 1921.

Kössl, M., and M. Vater. 1995. Cochlear structure and function in bats. Pages 191–234 *in*Hearing by bats. Springer.

Land, M. F., and D.-E. Nilsson. 2012. Animal eyes. Oxford University Press.

Leiser-Miller, L. B., and S. E. Santana. 2020. Morphological diversity in the sensory system of Phyllostomid bats: Implications for acoustic and dietary ecology. Functional Ecology 34:1416–1427.

Marroig, G., L. T. Shirai, A. Porto, F. B. de Oliveira, and V. De Conto. 2009. The Evolution of Modularity in the Mammalian Skull II: Evolutionary Consequences. Evolutionary Biology 36:136–148.

McCoy, D. E., and C. A. Norris. 2012. The cranial anatomy of the Miocene notoungulate Hegetotherium mirabile (Notoungulata, Hegetotheriidae) with preliminary observations on diet and method of feeding. Bulletin of the Peabody Museum of Natural History 53:355–374.

Meade, A., and M. Pagel. 2016. BayesTraits V3 81.

Monteiro, L. R., and M. R. Nogueira. 2010. Adaptive radiations, ecological specialization, and the evolutionary integration of complex morphological structures. Evolution 64:724–744.

Müller, B., S. M. Goodman, and L. Peichl. 2007. Cone photoreceptor diversity in the retinas of fruit bats (Megachiroptera). Brain, Behavior and Evolution 70:90–104.

Müller, B., and L. Peichl. 2005. Retinal cone photoreceptors in microchiropteran bats. Investigative Ophthalmology & Visual Science 46:2259.

Neaux, D., B. Blanc, K. Ortiz, Y. Locatelli, F. Laurens, I. Baly, C. Callou, et al. 2021. How changes in functional demands associated with captivity affect the skull shape of a wild boar (Sus scrofa). Evolutionary Biology 48:27–40.

772 Nogueira, M. R., L. R. Monteiro, A. L. Peracchi, and A. F. B. de Araújo. 2005. Ecomorphological
773 analysis of the masticatory apparatus in the seed-eating bats, genus Chiroderma (Chiroptera:
774 Phyllostomidae). Journal of Zoology 266:355–364.
775 Nogueira, M. R., A. L. Peracchi, and L. R. Monteiro. 2009. Morphological correlates of bite force
776 and diet in the skull and mandible of phyllostomid bats. Functional Ecology 23:715–723.
777 Paton, D. C., and B. G. Collins. 1989. Bills and tongues of nectar-feeding birds: A review of
778 morphology, function and performance, with intercontinental comparisons. Australian Journal
779 of Ecology 14:473–506.
780 Pedersen, S. C. 1993. Cephalometric correlates of echolocation in the Chiroptera. Journal of
781 Morphology 218:85–98.
782 ———. 1998. Morphometric analysis of the chiropteran skull with regard to mode of
783 echolocation. Journal of Mammalogy 79:91–103.
784 Porto, A., F. B. de Oliveira, L. T. Shirai, V. De Conto, and G. Marroig. 2009. The Evolution of
785 Modularity in the Mammalian Skull I: Morphological Integration Patterns and Magnitudes.
786 Evolutionary Biology 36:118–135.
787 Revell, L. J., L. J. Harmon, and D. C. Collar. 2008. Phylogenetic signal, evolutionary process, and
788 rate. Systematic Biology 57:591–601.
789 Rodriguez-Durán, A., and J. Rosa. 2020. Remarkable Variation in the Diet of Noctilio leporinus in
790 Puerto Rico: the Fishing Bat Turns Carnivorous. Acta Chiropterologica 22:175–178.
791 Rojas, D., O. M. Warsi, and L. M. Dávalos. 2016. Bats (Chiroptera: Noctilionoidea) challenge a
792 recent origin of extant neotropical diversity. Systematic Biology 65:432–448.

793 Rolfe, A. K. 2011. Diet of three mormoopid bats (Mormoops blainvillei, Pteronotus quadridens,
794 and Pteronotus portoricensis) on Puerto Rico.
795 Rossoni, D. M., B. M. A. Costa, N. P. Giannini, and G. Marroig. 2019. A multiple peak adaptive
796 landscape based on feeding strategies and roosting ecology shaped the evolution of cranial
797 covariance structure and morphological differentiation in phyllostomid bats. Evolution 73:1–57.
798 Sadier, A., K. T. J. Davies, L. R. Yohe, K. Yun, P. Donat, B. P. Hedrick, E. R. Dumont, et al. 2018.
799 Multifactorial processes underlie parallel opsin loss in neotropical bats. Elife 7:e37412.
800 Santana, S. E., E. R. Dumont, and J. L. Davis. 2010. Mechanics of bite force production and its
801 relationship to diet in bats. Functional Ecology 24:776–784.
802 Santana, S. E., I. R. Grosse, and E. R. Dumont. 2012. Dietary hardness, loading behavior, and the
803 evolution of skull form in bats. Evolution 66:2587–2598.
804 Santana, S. E., and S. E. Lofgren. 2013. Does nasal echolocation influence the modularity of the
805 mammal skull? Journal of Evolutionary Biology 26:2520–2526.
806 Teeling, E. C., S. C. Vernes, L. M. Davalos, D. A. Ray, M. T. P. Gilbert, E. Myers, Bat1K
807 Consortium, et al. 2018. Bat Biology, Genomes, and the Bat1K Project: To Generate
808 Chromosome-Level Genomes for All Living Bat Species. Annual Review of Animal Biosciences
809 6:23–46.
810 Thiagavel, J., C. Cechetto, S. E. Santana, L. Jakobsen, E. J. Warrant, and J. M. Ratcliffe. 2018.
811 Auditory opportunity and visual constraint enabled the evolution of echolocation in bats.
812 Nature Communications 9.
813 van der Meij, M. A. A., and R. G. Bout. 2008. The relationship between shape of the skull and
814 bite force in finches. Journal of Experimental Biology 211:1668–1680.

Vater, M., and M. Kössl. 2011. Comparative aspects of cochlear functional organization in mammals. Hearing Research 273:89–99.

Veilleux, C. C., and E. C. Kirk. 2014. Visual acuity in mammals: effects of eye size and ecology. Brain, Behavior and Evolution 83:43–53.

Wagner, G. P., and L. Altenberg. 1996. Perspective: complex adaptations and the evolution of evolvability. Evolution 50:967–976.

Warton, D. I., R. A. Duursma, D. S. Falster, and S. Taskinen. 2012. smatr 3--an R package for estimation and inference about allometric lines. Methods in Ecology and Evolution 3:257–259.

Watanabe, A., A. C. Fabre, R. N. Felice, J. A. Maisano, J. Müller, A. Herrel, and A. Goswami. 2019. Ecomorphological diversification in squamates from conserved pattern of cranial integration. Proceedings of the National Academy of Sciences of the United States of America 116:14688–14697.

Watanabe, A., P. M. Gignac, A. M. Balanoff, T. L. Green, N. J. Kley, and M. A. Norell. 2018. Are endocasts good proxies for brain size and shape in archosaurs throughout ontogeny? Journal of Anatomy.

Wiley, D. F., N. Amenta, D. A. Alcantara, D. Ghosh, Y. J. Kil, E. Delson, W. Harcourt-Smith, et al. 2005. Evolutionary morphing. IEEE.

Winter, Y., and O. von Helversen. 2003. Operational tongue length in phyllostomid nectar-feeding bats. Journal of Mammalogy 84:886–896.

Yohe, L. R., M. Fabbri, D. Lee, K. Davies, T. P. Yohe, M. K. Sanchez, E. Rengifo, et al. 2021. Ecological constraints on highly evolvable olfactory receptor genes and morphology. bioRxiv.

836 Yohe, L. R., S. Hoffmann, and A. Curtis. 2018. Vomeronasal and olfactory structures in bats
837 revealed by DiceCT clarify genetic evidence of function. Frontiers in Neuroanatomy 12:32.
838
839 **Table and Figure Captions**
840
841 **Table 1:** Results from major axis regression comparing the observed variance - rate
842 relationships to the relationship predicted under Brownian motion evolution of uncorrelated
843 traits. Type indicates the Brownian Motion null (BM), sensory modules (S) and mechanical
844 modules (M). Results with p-values < 0.05 are in bold type.
845
846 **Figure 1:** Tree of sampled taxa color coded by feeding guild. Silhouettes appear in the same
847 sequence as the species in bold type. Phylogeny based on Rojas et al (2016).
848
849 **Figure 2:** Degree of integration within Noctilionoidea and its subdivision into phyllostomids and
850 other noctilionoids. Within-module integration (diagonal values) and between-module
851 integration (off-diagonal values) are expressed as Rho coefficients (ρ) and calculated using
852 EMMLi. Integration among mechanical modules is in the blocks above the horizontal black lines
853 and integrations among the sensory modules are in the blocks to the left of the vertical black
854 lines. The group of blocks delineated by the black lines describes the integration between
855 mechanical and sensory modules. Hotter colors represent higher integration.
856
857 **Figure 3:** Evolutionary rate of each module is plotted against time for sensory modules (top)

and mechanical modules (bottom). Vertical lines denote the location of nodes associated with positively selected visual genes (Davies et al 2020): the ancestor of Mormoopidae (M), the ancestor of Noctilionidae (N), the ancestor of Phyllostomidae (P), the origin of plant-feeding within phyllostomids (Plt), the ancestor of the nectar-feeding Glossophaginae (G), the ancestor of the nectar-feeding Lonchophyllinae (L), and the ancestor of the fig-eating Stenodermatinae (S).

Figure 4: Evolutionary rates of each module mapped onto the phylogeny. Branch lengths are scaled by rates of evolution. Cool colors indicate low rates and warm colors indicate high rates. The red star indicates the origin of phyllostomids, orange stars indicate the origins of nectarivory and the black star indicates origin of the fig-eating stenodermatines. A-C are sensory modules, E is a time-calibrated phylogeny, and D and F-I are mechanical modules.

Figure 5: Maps of PC1 and PC2 of olfactory bulb and palate module shapes across noctilionoids.

Figure 6: Relationships among average disparity (Procrustes variance), rate (σ^2Rate) of evolution and integration (ρ).

S1 Figure: Illustration of hypothesized modules with landmarks to represent their shapes

S1 – 6 Figures: Maps of PC1 and PC2 of shape for the eye, cochlea, cranial base, face, external vault, and zygomatico-glenoid modules across noctilionoids.

S1 Table: Sampled specimens and their museum accession numbers.

S2 Table: Landmarks used and their descriptions.

S3 Table: Sensitivity tests of down-sampled landmarks.

S4 Table: Hypothesized modules in bat skulls using 3D landmark coordinates from internal surface, external surface, and eye orbits.

S5 Table: Modularity tests (EMMLi output) using various combinations of partitions in bat crania. The best supported model is shown in bold font.

S6 Table: Net rates of evolution of modules for each of phyllostomids and non-phyllostomid noctilionoids and pairwise comparisons of these (first for the whole Noctilionoidea by each group).

S7 Table: Pairwise comparisons in the disparity - rate slopes across modules (for the complete Neotropical Noctilionoidea group sampled, then phyllostomids alone, and non-phyllostomid noctilionoids).

S8 Table: Regression of ρ coefficient of each module against the number of landmarks within each module

S9 Table: EMMLi results after reducing the number of landmarks on the eye to seven (one in the center and one on each pole) – Same as obtained using the full 55.

S1 Video: Landmark points mapped onto the skull of *Uroderma bilobatum* showing five modules (Eye, External Vault, Palate, Face, Zygomatico-glenoid complex) and part of the Base

S2 Video: Landmark points mapped onto the skull of *Erophylla bombifrons* showing three modules Cochlea, Olfactory bulb, and the Base

Acknowledgements

We would like to thank Greg Lin and Jim Reynolds for access to the µCT scanner used in this study and for technical support. This work was performed in part at the Center for Nanoscale Systems (CNS), a member of the National Nanotechnology Coordinated Infrastructure Network, which is supported by the National Science Foundation under award number ECS 1541959. For access to specimens, we would like to thank the American Museum of Natural History and the Yale Peabody Museum. We would like to thank Ryan Felice and Robin Trayler for help with R coding. This project was made possible by funding from the National Science Foundation (PRFB-1612211, DEB-1442142, DEB-1442314, and DEB-1442278).

Figure 1

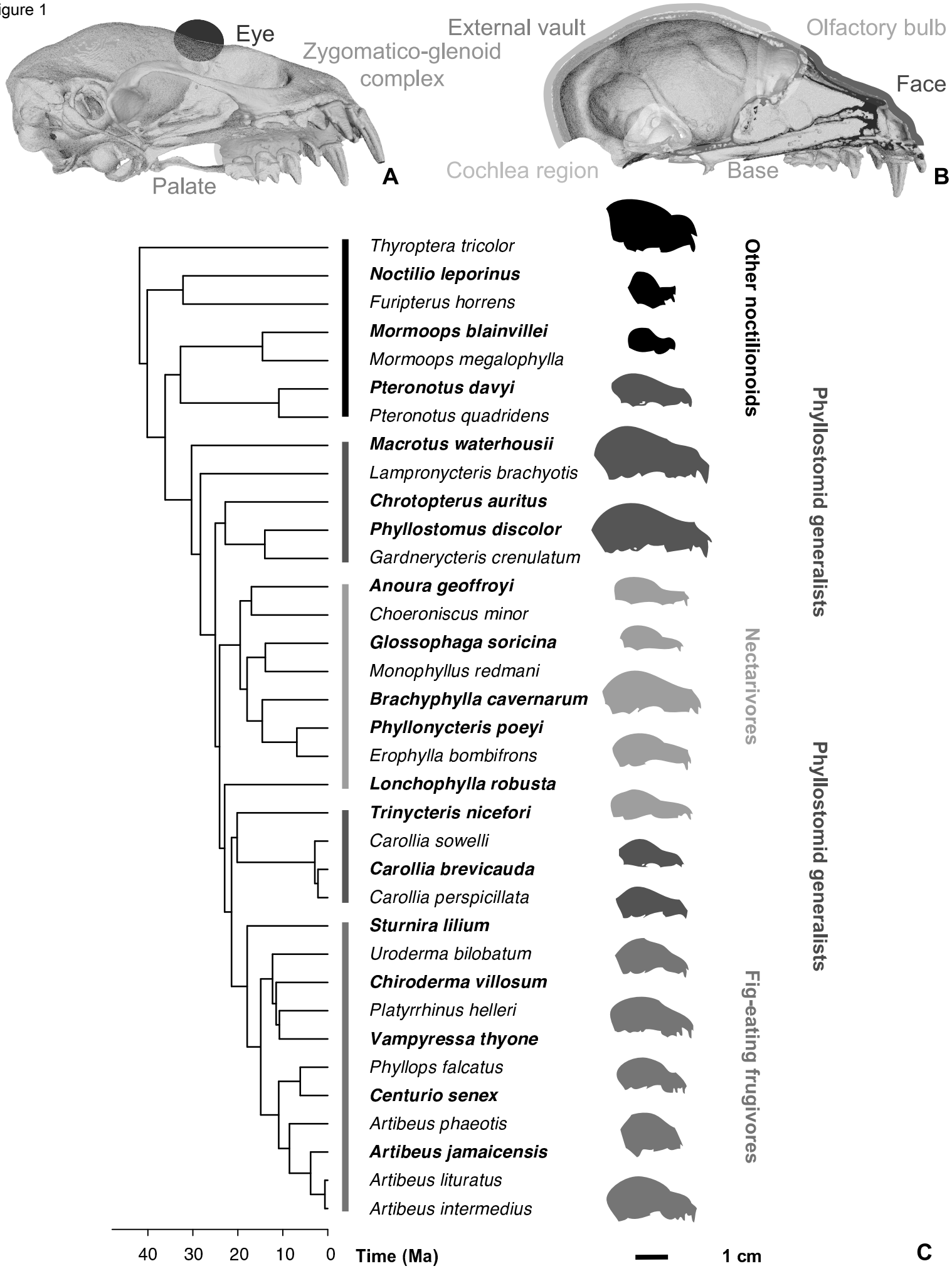
Eye
Zygomatico-glenoid complex
Palate
A
External vault
Olfactory bulb
Face
Cochlea region
Base
B
Thyroptera tricolor
Noctilio leporinus
Furipterus horrens
Mormoops blainvillei
Mormoops megalophylla
Pteronotus davyi
Pteronotus quadridens
Macrotus waterhousii
Lampronycteris brachyotis
Chrotopterus auritus
Phyllostomus discolor
Gardnerycteris crenulatum
Anoura geoffroyi
Choeroniscus minor
Glossophaga soricina
Monophyllus redmani
Brachyphylla cavernarum
Phyllonycteris poeyi
Erophylla bombifrons
Lonchophylla robusta
Trinycteris nicefori
Carollia sowelli
Carollia brevicauda
Carollia perspicillata
Sturnira lilium
Uroderma bilobatum
Chiroderma villosum
Platyrrhinus helleri
Vampyressa thyone
Phyllops falcatus
Centurio senex
Artibeus phaeotis
Artibeus jamaicensis
Artibeus lituratus
Artibeus intermedius
Other noctilionoids
Phyllostomid generalists
Nectarivores
Phyllostomid generalists
Fig-eating frugivores
40
30
20
10
0
Time (Ma)
1 cm
C

Figure 2

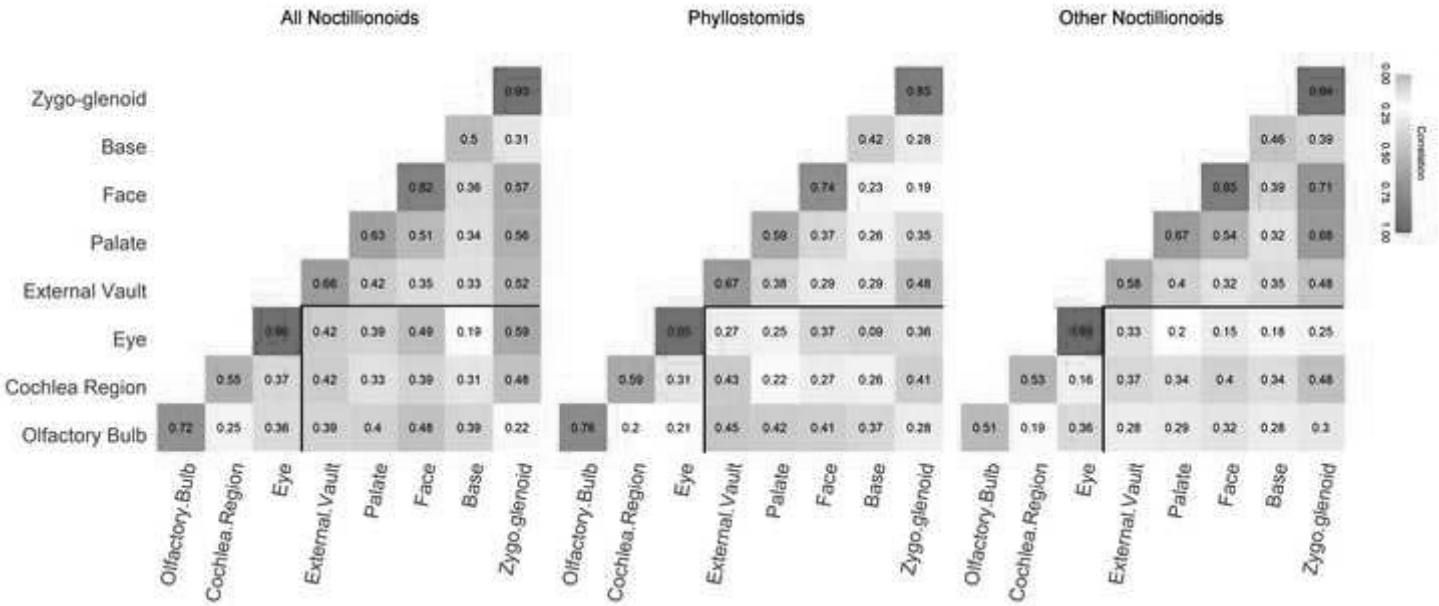
All Noctillionoids
Phyllostomids
Other Noctillionoids
Zygo-glenoid
Base
Face
Palate
External Vault
Eye
Cochlea Region
Olfactory Bulb
Olfactory.Bulb
Cochlea.Region
Eye
External.Vault
Palate
Face
Base
Zygo.glenoid
Correlation

Figure 3

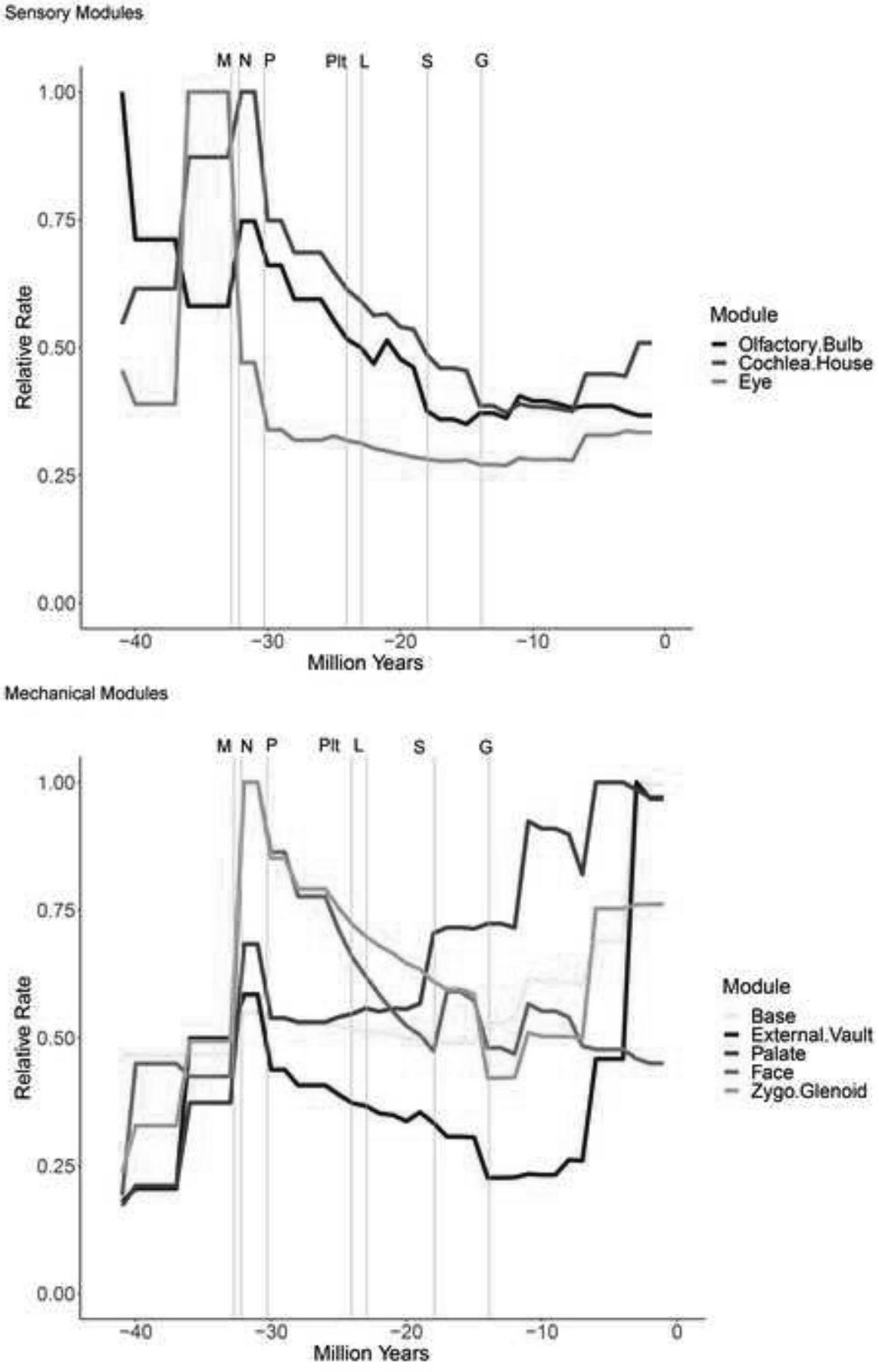
Sensory Modules
M N P Plt L S G
1.00
0.75
0.50
0.25
0.00
Relative Rate
−40
−30
−20
−10
0
Million Years
Module
Olfactory.Bulb
Cochlea.House
Eye
Mechanical Modules
M N P Plt L S G
1.00
0.75
0.50
0.25
0.00
Relative Rate
−40
−30
−20
−10
0
Million Years
Module
Base
External.Vault
Palate
Face
Zygo.Glenoid

Figure 4


Slow
Fast
Olfactory Bulb
Cochlea
Eye
A
B
C
Underlying Phylogeny
Face
Palate
Thyroptera tricolor
Noctilio leporinus
Furipterus horrens
Mormoops blainvillei
Mormoops megalophylla
Pteronotus davyi
Pteronotus quadridens
Macrotus waterhousii
Lampronycteris brachyotis
Chrotopterus auritus
Phyllostomus discolor
Gardnerycteris crenulatum
Anoura geoffroyi
Choeroniscus minor
Glossophaga soricina
Monophyllus redmani
Brachyphylla cavernarum
Phyllonycteris poeyi
Erophylla bombifrons
Lonchophylla robusta
Trinycteris nicefori
Carollia sowelli
Carollia brevicauda
Carollia perspicillata
Sturnira lilium
Uroderma bilobatum
Chiroderma villosum
Platyrrhinus helleri
Vampyressa thyone
Phyllops falcatus
Centurio senex
Artibeus phaeotis
Artibeus jamaicensis
Artibeus lituratus
Artibeus intermedius
D
E
F
Zygomatic–Glenoid Complex
Skull Base
External Vault
G
H
I

Figure 5

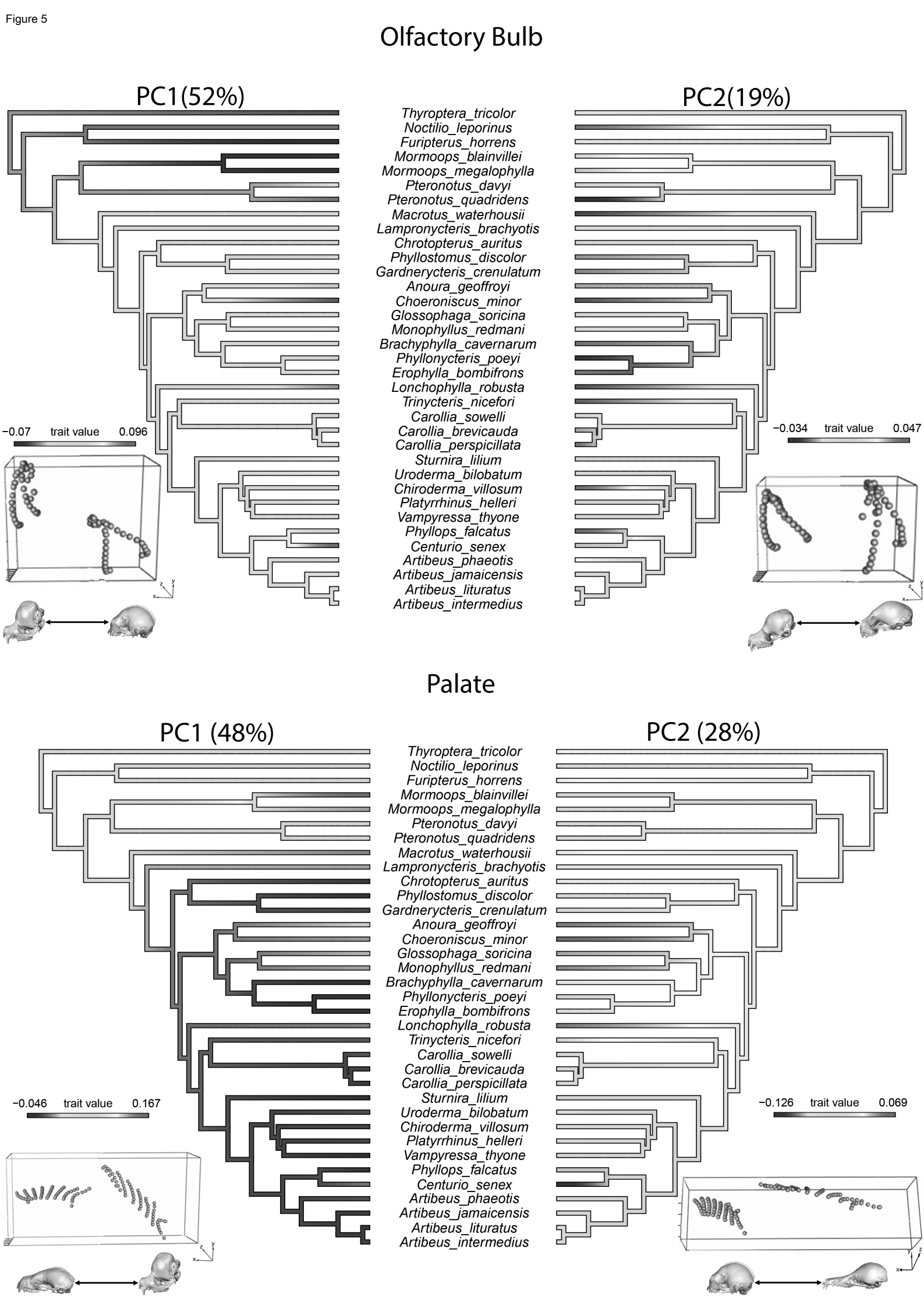
Olfactory Bulb
PC1(52%)
PC2(19%)
Thyroptera_tricolor
Noctilio_leporinus
Furipterus_horrens
Mormoops_blainvillei
Mormoops_megalophylla
Pteronotus_davyi
Pteronotus_quadridens
Macrotus_waterhousii
Lampronycteris_brachyotis
Chrotopterus_auritus
Phyllostomus_discolor
Gardnerycteris_crenulatum
Anoura_geoffroyi
Choeroniscus_minor
Glossophaga_soricina
Monophyllus_redmani
Brachyphylla_cavernarum
Phyllonycteris_poeyi
Erophylla_bombifrons
Lonchophylla_robusta
Trinycteris_nicefori
Carollia_sowelli
Carollia_brevicauda
Carollia_perspicillata
Sturnira_lilium
Uroderma_bilobatum
Chiroderma_villosum
Platyrrhinus_helleri
Vampyressa_thyone
Phyllops_falcatus
Centurio_senex
Artibeus_phaeotis
Artibeus_jamaicensis
Artibeus_lituratus
Artibeus_intermedius
−0.07 trait value 0.096
−0.034 trait value 0.047
Palate
PC1 (48%)
PC2 (28%)
−0.046 trait value 0.167
−0.126 trait value 0.069

Figure 6

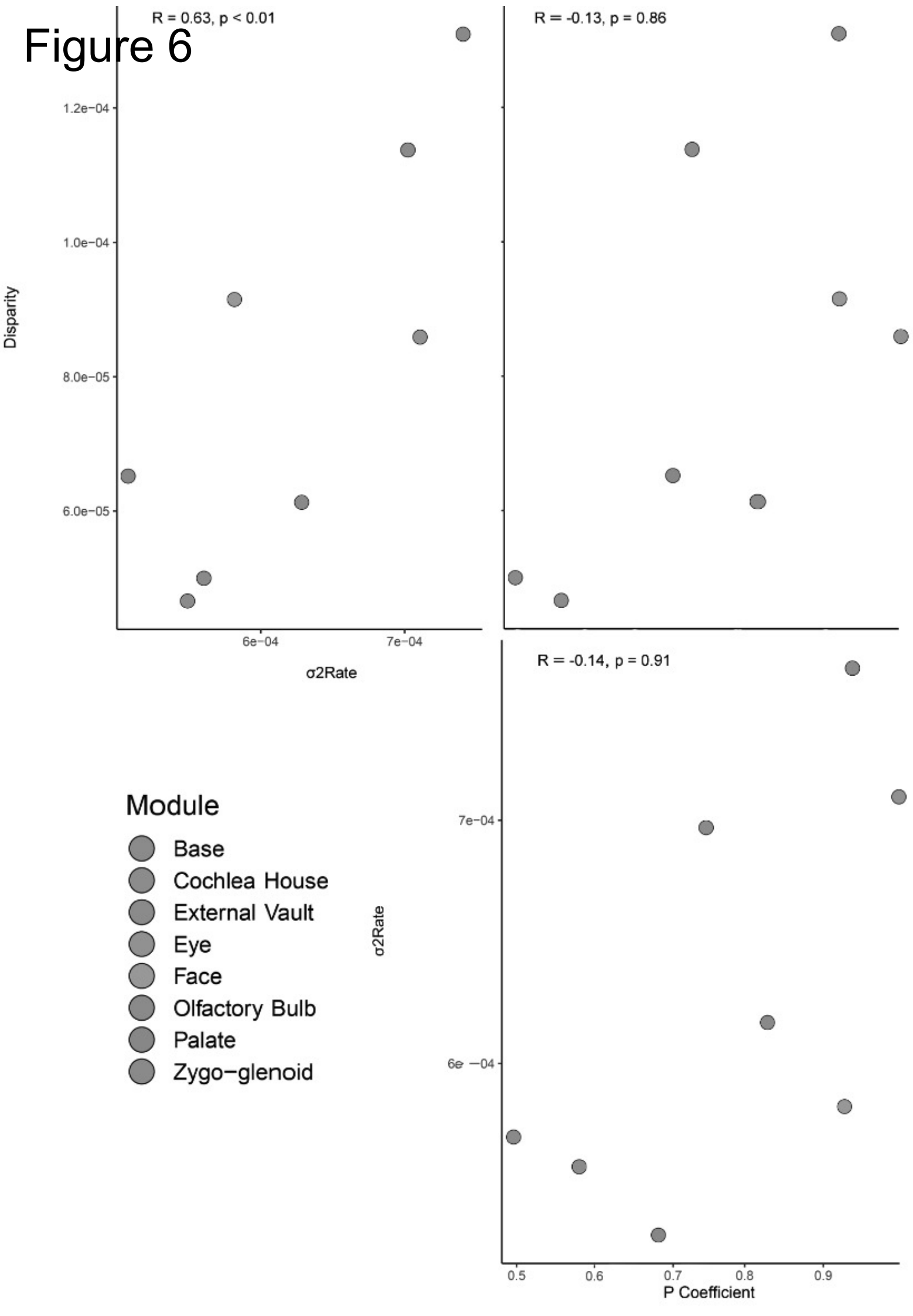
R = 0.63, p < 0.01
R = -0.13, p = 0.86
R = -0.14, p = 0.91
Disparity
σ2Rate
P Coefficient
1.2e−04
1.0e−04
8.0e−05
6.0e−05
7e−04
6e−04
0.5
0.6
0.7
0.8
0.9
Module
Base
Cochlea House
External Vault
Eye
Face
Olfactory Bulb
Palate
Zygo−glenoid

Data for Repository

Click here to download Data for Repository
https://datadryad.org/stash/share/nAJrvN7DKFny4khK92FR-

Supplementary Figure 1

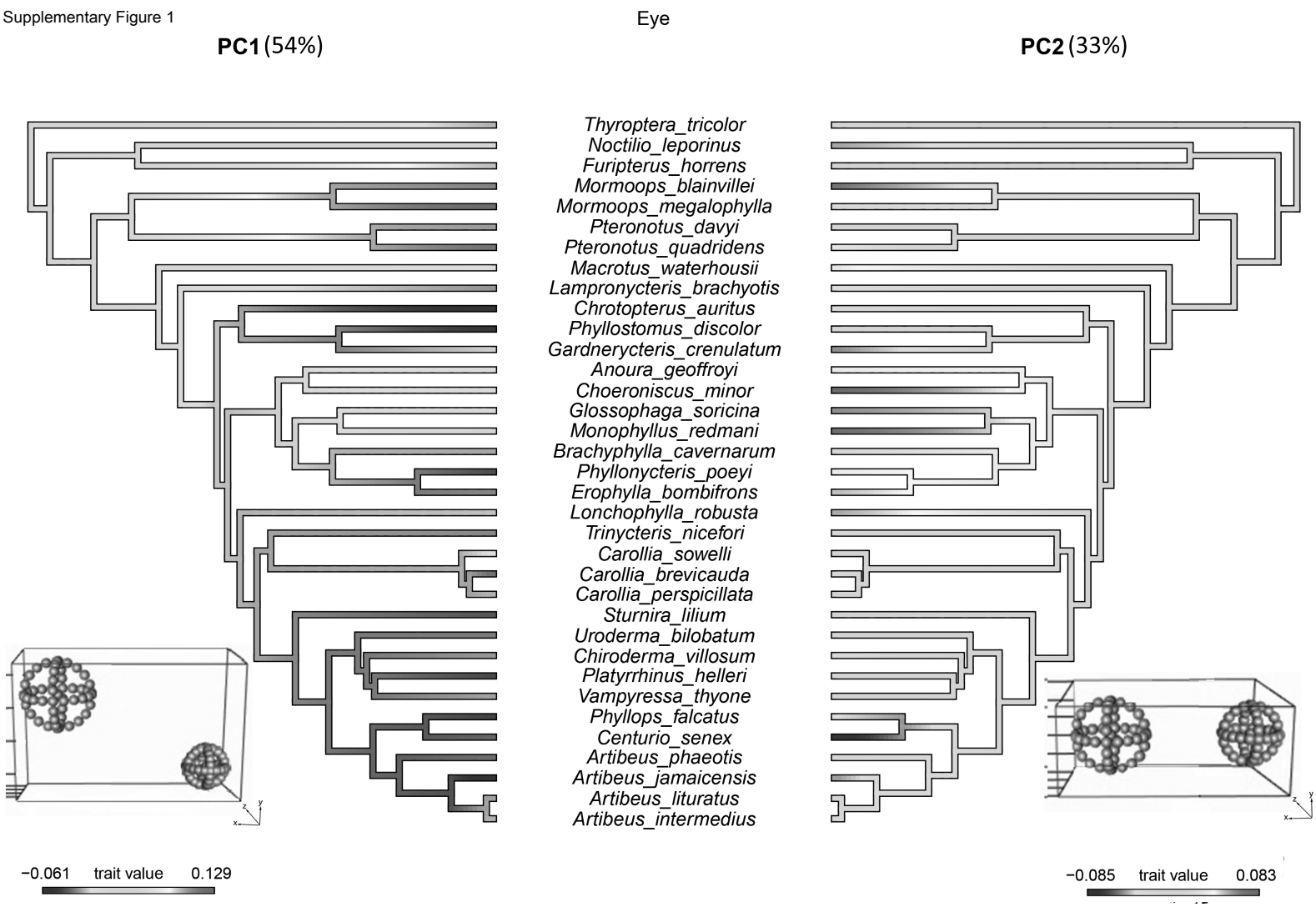

Supplementary Figure 2

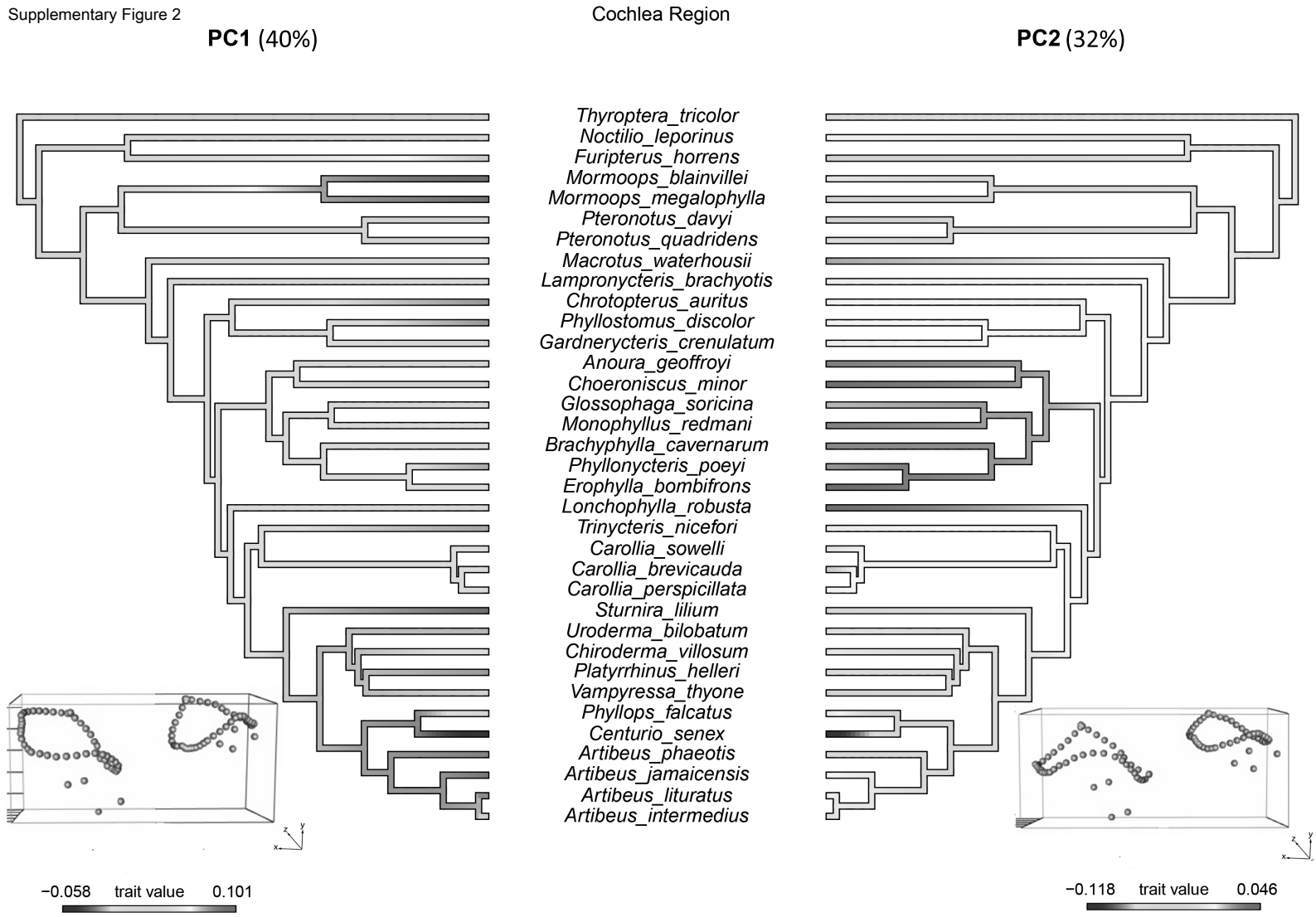

Supplementary Figure 3

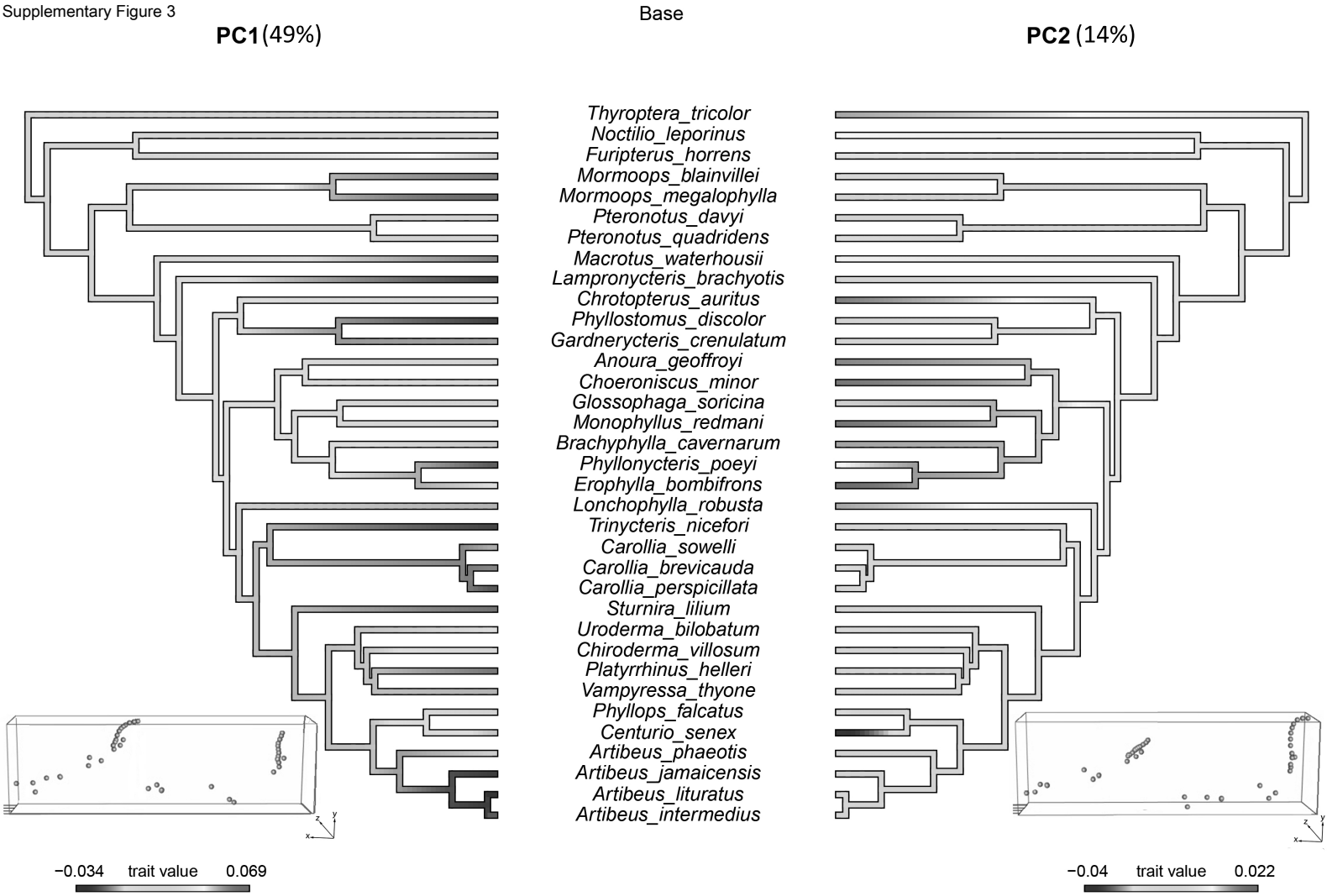

Supplementary Figure 4

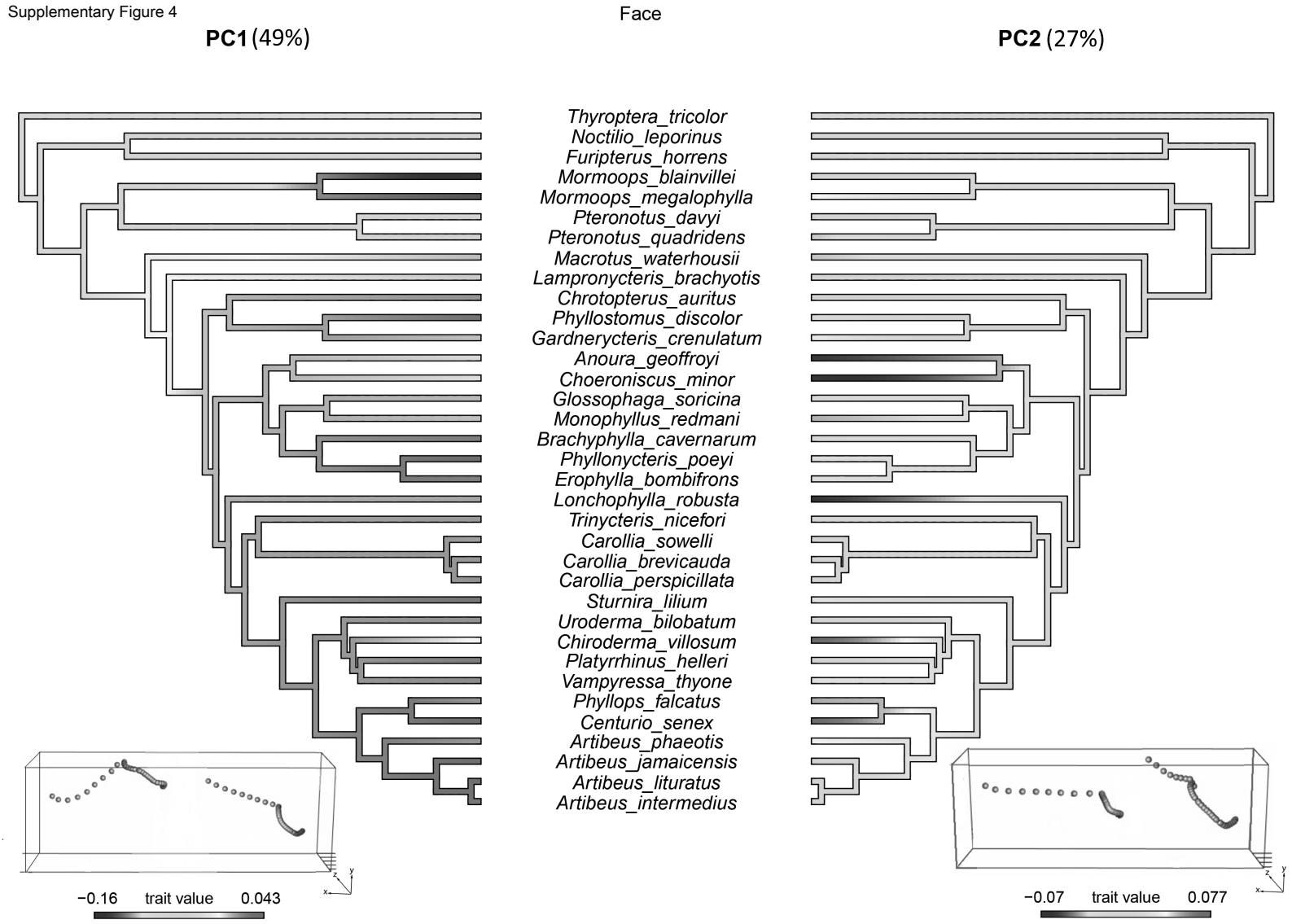

Supplementary Figure 5

External Vault

PC1 (54%)

PC2 (31%)

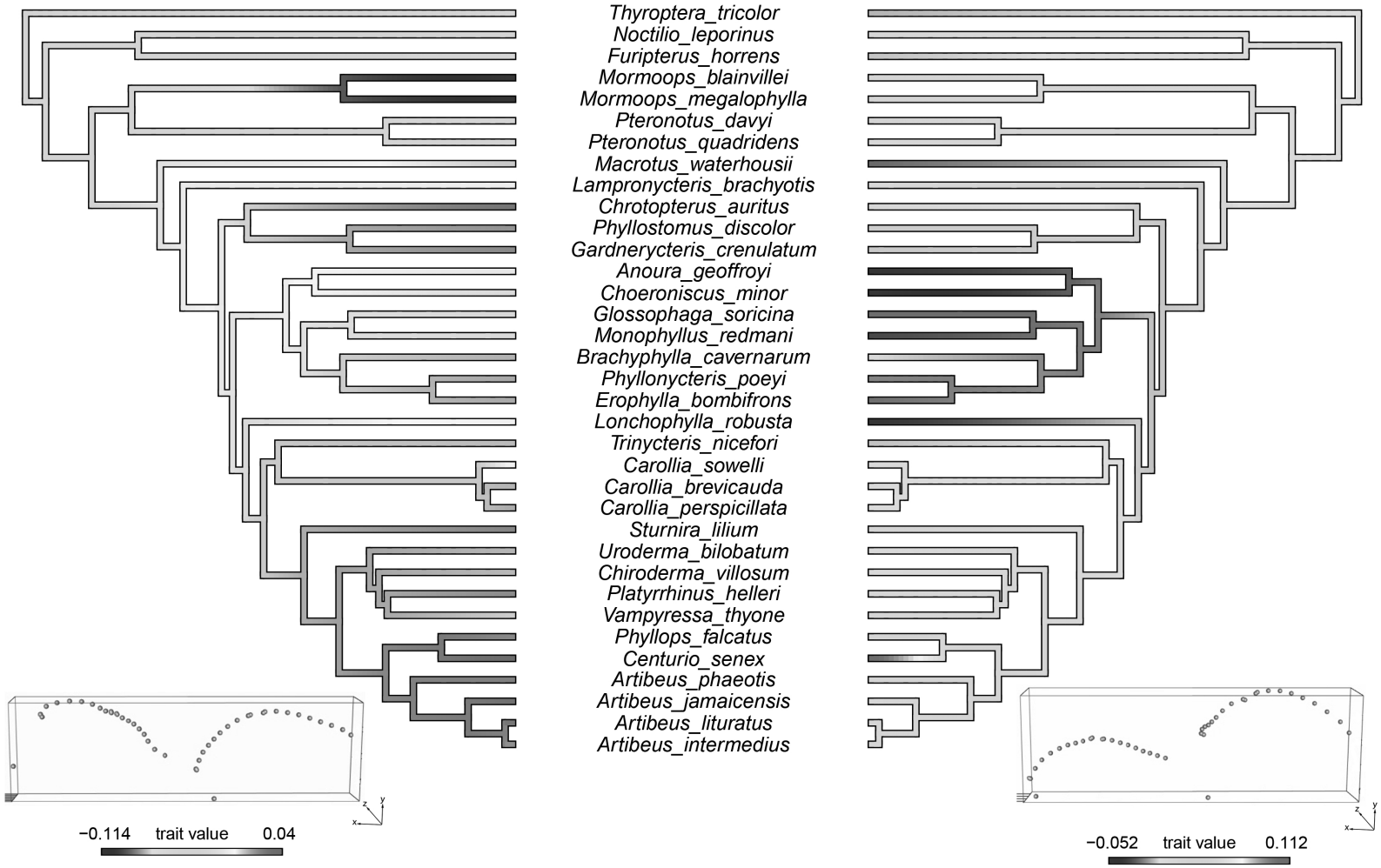

Supplementary Figure 6

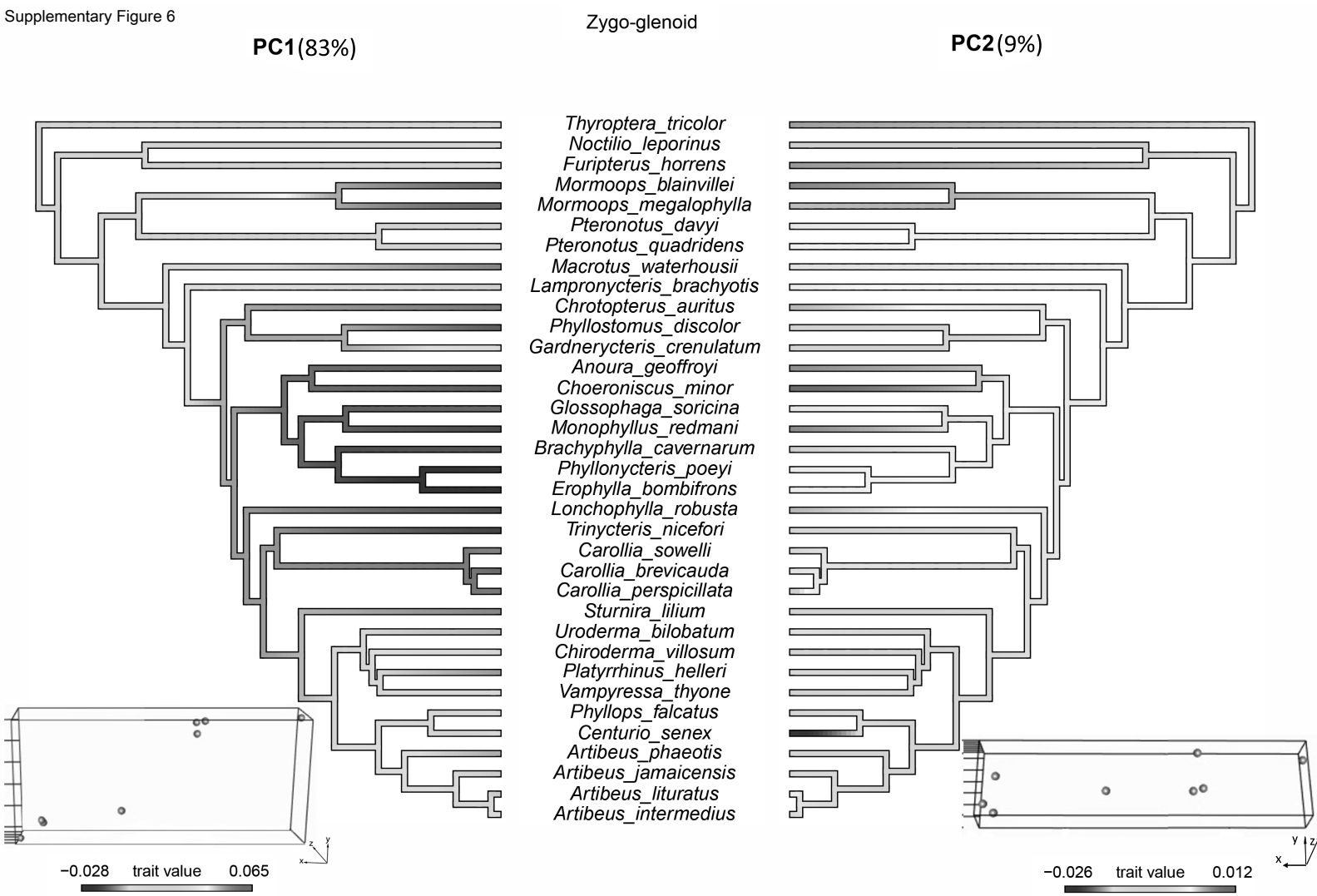

Supplementary Video 1

Click here to access/download

Other Supplements (Video, Excel, large figure files)

S1 Video.mp4

Supplementary Video 2

Click here to access/download

Other Supplements (Video, Excel, large figure files)

S2 Video.mp4